Report research Molecular Systems Biology

MSc Research Project 1
Sietse Couperus
S4093410
Supervisors: Andreas Milias-Argeitis, Andriana Koutsoumpa
25 March 2022

Contents

Introduction

The cell cycle is one of the most fundamental processes in biology. Every organism must grow and divide, so every organism goes through the cell cycle. Since the cell cycle is such a fundamental process, it is highly conserved among organisms. For this reason, knowledge gained about the cell cycle of one species can be applied to that of humans. The cell cycle is central to the proliferation of cells during fetal development and the regeneration of tissues. Disruptions of these processes can lead to incomplete proliferation or uncontrolled proliferation, i.e. cancer (Venkitaraman, 2002). Therefore, a thorough understanding of the processes of the cell cycle is vital to combat developmental disorders and cancer. Budding yeast is an easily grown model organism that is used to investigate the cell cycle. Its ease of cultivation and the large genetic modification toolkit make this an attractive organism to study the processes of the cell cycle that would be infeasible to study with human cells only.

The cell cycle is divided into interphase and mitosis. During interphase, the cell grows, duplicates its DNA and forms a bud while during mitosis the cell divides all its contents between the daughter cells. The first part of the interphase is the G_1 phase, during which the cell grows and produces protein (Morgan, 2007). At the end of this phase the cell goes through a checkpoint called START. The START checkpoint determines whether the cell will commit to cell division and progress into the next phase, the S phase, of the cell cycle (Hartwell & Weinert, 1989). In the S phase the DNA of the cell is replicated and then the cell progresses to the second growth phase of the cell, G_2 (Morgan, 2007). At the end of the G_2 phase another checkpoint must be passed to check if the DNA is not damaged (Sha, Moore & Chen, 2002). After this checkpoint the cell enters the mitotic (M) phase during which the mother and daughter cells separate and the cell cycle begins anew. The progression of the cell cycle is governed by cyclins and cyclin-dependent kinase 1 (Cdk1) (Morgan, 2007). Cyclins bind to the cyclin-dependent kinase and direct its kinase activity towards specific targets. The cyclin-Cdk1 complex then phosphorylates these targets, which go on to activate certain cell cycle processes (Morgan, 2007). In budding yeast, some parts of the cell cycle progression can be performed by a single cyclin, showing that there is some redundancy in the system, but other parts of the cell cycle cannot be performed without all sets of cyclins (Ercan *et al*., 2021). This shows that each set of cyclins have their specific functions and the cyclins perform these functions by directing Cdk1 towards different targets and thus activating different parts of the cell cycle.

The transition from the G_1 phase to the S phase via the START checkpoint in yeast is driven by the G_1/S cyclins Cln1 and Cln2. During the G_1 phase the Whi5 protein binds to the SBF and MBF transcription factors, which inhibits their activity. These transcription factors control Cln1 and Cln2 expression. The G_1 cyclin Cln3 phosphorylates Whi5 which leads to its dissociation from SBF and the subsequent transcription of Cln1 and Cln2 (Costanzo *et al*., 2004*;* de Bruin *et al*., 2004). Cln1 and Cln2 also direct Cdk1 to phosphorylate Whi5 which leads Whi5 to exit the nucleus and forms a positive feedback loop that ensures that the START checkpoint is irreversible (Skotheim *et al*., 2008). Deletion of Cln3 was shown to increase the variability of the G_1 phase duration while the deletion of Swi4, which is part of SBF that activates Cln2 expression, leads to decoherence of START and mistiming of several S phase processes (Bean *et al.,* 2006). While any combined deletion of two Cln proteins is still viable, the deletion of all three Cln proteins lead to full cell cycle arrest and are therefore not viable (Edgington & Futcher, 2001). The irreversible effect of Cln1 and Cln2 on cell cycle progression, amplified by the

positive feedback loop, make the G_1/S cyclins prime targets to artificially alter the cell cycle to facilitate study of cellular processes (Charvin *et al*., 2009; Perrino *et al*., 2021. The cln1 and Cln2 proteins also have a role outside of the nucleus. They are involved in morphogenesis of the bud neck and the disruption of Cln1 or Cln2 leads to a misshapen bud neck (Gladfelter *et al.*, 2005). Both the nuclear and cytoplasmic roles of Cln2 are essential to cell functioning, which is shown by the inability of Cln2 to rescue the *cln1, cln2, cln3* mutant phenotype when localized exclusively either inside the nucleus or outside the nucleus (Edgington & Futcher, 2001). Cln1 and Cln2 are also involved in bud formation and spindle pole formation. Removing these proteins was shown to disrupt these processes (McCusker *et al*., 2007).

While many effects of Cln2 have been reported, most work done so far has been qualitative and a thorough quantitative characterization of strains with various levels of Cln2 expression is lacking. This lack is caused mainly by a lack of high throughput, detailed data collection techniques. One problem with cell cycle research leading to this lack of large amounts of detailed data is that of cell heterogeneity. In a yeast culture, not all cells are in the same phase of the cell cycle. Moreover, synchronized cells will become desynchronized after roughly two cell cycles without any additional control (Perrino *et al*., 2021). For this reason, a culture of yeast cells has limited value when researching the cell cycle since all measurements will yield a population average, which will contain limited information about the temporal dynamics of the cell cycle. Asserting full control of the G_1 and G_1/S cyclins would make it possible to stop the cell cycle at will and synchronize the cell cycle of an entire yeast culture. Previous research has used chemical induction, but chemical inducers cannot be easily removed from a liquid culture (Perrino *et al*., 2021). An alternative approach is the use of optogenetics. Light-sensitive proteins can be switched on or off rapidly in response to light which allows for more control of the transcription of the target protein (Rullan *et al*., 2018). Beyond cell cycle synchronization, optogenetic control of the cell cycle could be used to study the cell cycle at the single cell level, possibly in combination with other mutations.

For these reasons an optogenetic system that can control the cell cycle has been long sought after. In this study, two strains are constructed with optogenetically activated Cln2 in order to produce a yeast strain whose cell cycle can be speed up or slowed down through the input of light. These strains had a cln2,3Δ background with Cln2 placed in a non-endogenous locus under the control of an optogenetic system to alter the expression of Cln2. Cln2 was chosen as the target instead of Cln1 because while the two proteins are redundant, deletion of Cln2 was shown to have a larger effect on the cell cycle and cell morphology than deletion of Cln1 (Queralt & Igual, 2004). The Cln3 protein was also removed since Cln3 and Cln1 together are sufficient to pass the START transition, so the regulation of Cln2 would have little effect on the cells. Since a cln1,2,3Δ strain is not viable, Cln1 was left unaltered. These strains were observed under the microscope and the effects of light stimulation on the cell cycle and cell morphology were quantified. The YeaZ convolutional neural network was used to track single cells in the microscopy images (Dietler *et al*., 2020). Convolutional neural networks are specialized in image recognition and use simple features to recognize more complex objects (LeCun *et al*., 1998). The network outputs a mask for each cell it recognizes in an image and this can be used to calculate certain properties of the cell (Van Valen *et al*., 2018). The use of a neural network allowed for the rapid quantification of the G1 duration and cell size of a large number of cells. This data was used for a quantitative analysis of the effects of the optogenetically regulated Cln2 construct on the cell cycle and

cell morphology. In the first experiments cells were grown under constant light or dark conditions, to determine the range of Cln2 expression that this system could achieve. Transitions from light-to-dark and dark-to-light conditions were then used to determine the ability of the optogenetic system to influence cell cycle dynamics and respond rapidly to light inputs. In addition, a small and easy-to-use turbidostat from Chi.Bio was set up to determine the growth rate of these strains with fine temporal detail under different lighting conditions. The turbidostats can gather more data per run, require less manual operation than a traditional turbidostat set up, and can be run with multiple vessels in parallel (Steel *et al*., 2019). This data was used to complete the characterization of the optogenetically activated Cln2 strains and confirm the alterations of the cell cycle duration in response to light that was observed under the microscope. Lastly, the effects of the Cln2 perturbation on cell death and growth arrest was quantified. Cells were observed to die or stop growing in the Cln2 mutant strains and therefore, the occurrence was quantified in each strain and lighting condition to determine whether this is caused by the optogenetic switching of Cln2 expression. These experiments result in two *S. cerevisiae* strains that show differential behaviour based on lighting conditions. One of the strains displays on-switching behaviour, but none of the two strains can switch off after being activated. These two strains are a step forward in constructing a fully tunable Cln2 construct and provide insights into the issues still needing to be resolved.

Materials and Methods

Microscopy

The strains were incubated overnight in YNB + 2% glucose at 30 °C and 300 rpm. The next day, the cells were diluted to OD_{600} 0.2 in YNB + 2% glucose and grown until the OD_{600} was 0.7. During this precultivation the flasks were covered with an aluminium foil jacket to keep the cells in the dark. 2 µL of the cells was then placed on a microscope slide and covered with a cube of YNB agar. This slide was mounted in a metal holder and covered with another microscope slide to prevent moisture from evaporating during the experiment. The microscope slides were prepared in a dark room with only a red light source to avoid activation of EL222 by ambient light. The slides were carried in a cardboard box when being moved to avoid ambient light during transportation as well. The slides were viewed with an inverted fluorescence microscope (Eclipse Ti-E, Nikon Instruments) for several hours per experiment. Multiple positions on the slide were imaged per experiment and each position was imaged once every five minutes to create a time lapse of the growth of the cells. During the experiments the temperature of the slide was kept at 30 °C to allow the cells to grow normally using a microscope incubator (Life Imaging Services). The cells were imaged with an iXon Ultra 897 DU-897-U-CD0-#EX camera from Andor Technology through a 100x Nikon S Fluor objective (N.A. = 1.30). The EL222 system was activated with a 400 nm laser for stimulating CFP set at 1% intensity laser and 1 second exposure time. The Whi5-mCherry was excited with an 565 nm laser at 50% intensity and 1 second exposure time. The Cln2-mNG was excited with a 470 nm laser at 70% intensity and 600 milliseconds exposure time.

Construction of pFA6-GAL(UAS)-EL222(5xBS)-prGAL1-Cln2-mNG

A plasmid was made from the pFA6 backbone, an upstream sequence of GAL1 required for expression, five EL222 binding sites, the GAL1 promoter and Cln2-mNeonGreen. The pFA6 backbone, a standardized plasmid for cloning in *E. coli*, contained an ampicillin resistance marker. The pFA6 backbone plasmid was already purified and linearized for Gibson assembly. The EL222(5xBS) and Cln2-mNG were amplified from the genomic DNA of strain 1 with the EL222_fwd and EL222_rev primers, and the Cln2_fwd and mNG_rev primers, respectively (**Supplementary information, Table S3**). The parts were amplified with the Q5 PCR protocol with an annealing temperature of 68 °C for EL222 and 69 °C for Cln2-mNG (**Supplementary information, Table S1 & S2**. The PCR products were run on a gel for 30 minutes with a voltage of 120 V to confirm the correct size of the PCR products. The expected band size was 190 bp for EL222 and 2391 bp for Cln2-mNG (**Supplementary information, Figure S1A & S1B**). Then the GAL1(UAS) was amplified using the GAL-UAS_fwd and GAL-UAS_rev primers. The prGAL1 part was also amplified from the genomic DNA of strain 1 with the Gal1_fwd and Gal1_rev primers (**Supplementary information, Table S3**) and an annealing temperature of 66 °C. The expected band size was 431 bp (**Supplementary information, Figure S1C**). The parts were amplified according to the Q5 PCR protocol with an annealing temperature of 68 °C. After the parts were amplified an attempt was made to put the five parts together using a Gibson assembly (**Supplementary information, Table S4**). After assembly competent DH5α cells were transformed with the resulting plasmid. The transformed cells were then grown and miniprepped to extract the amplified plasmid. The plasmid was then sequenced using the Gal1-seq primer to determine whether the Gibson assembly had produced the desired plasmid (**Supplementary information, Sequence 1**).

After sequencing showed that only Cln2-mNG and GAL(UAS) were assembled into the pFA6 backbone, the five-part Gibson assembly strategy was abandoned. Instead, new primers were designed to produce a Cln2-mNG-pFA6-GAL(UAS) fragment that overlapped with prGAL1 and EL222(5xBS) to reduce the number of parts to three (**Supplementary information, table S3**). The prGAL1 and EL222(5xBS) remained unchanged in this new strategy. The EL222(5xBS) and prGAL1 were inserted into the new backbone through a Gibson assembly (**Supplementary information, Table S5**). Inoue competent DH5α cells were transformed in duplo with the assembled plasmid and incubated for one day at 37 ^{o}C. From each plate 3 colonies were picked and miniprepped. The extracted plasmids were then sent for sequencing with the Gal1-seq primer (**Supplementary information, Table S3**). One of the plasmids was shown to have the correct sequence(**Supplementary information, Sequence 2**).

Yeast strain construction

A parental strain with cln2,3 deletion, the EL222 cassette in the HO locus and the Whi5-mCherry marker had already been constructed. This strain, yAK31.2.1 (**Table 2**), had the EL222(5xBS)-Spo13-Cln2-mNG or GAL1(UAS)-EL222(5xBS)-prGAL1-Cln2-mNG construct inserted into the X1 locus, producing the strains ySC3.1 and ySC4.1 (**Table 2**). The parental strain, which had already lost its previous CRISPR plasmid, was transformed with a CRISPR plasmid targeting the X1 locus and repair fragments to produce the two strains according to the protocol from Novarina *et al*. (2022). The CRISPR plasmid was built with the YTK plasmids from this protocol and contained a gRNA targeting the X1 locus and a nourseothricin resistance marker. The repair fragments contained the optogenetic Cln2 constructs and were flanked by upstream and downstream sequences of the X1 locus where the gRNA cuts (**Table 1**). A pFA6-EL222(5xBS)-prSpo13-Kozak-cln2-mNG plasmid that had been previously used for the construction of the yAK38.2.1 strain, was used to produce repair fragment 3 (RF3) (**Table 1**). RF3 was produced using the RF3_fwd and RF3_rev primers (**Supplementary information, Table S3**). The pFA6-GAL1(UAS)-EL222(5xBS)-prGAL1-Cln2-mNG plasmid was used to produce repair fragment 4 (RF4) (**Table 1**) using the RF4_fwd and RF4_rev primers (**Supplementary information, Table S3**). The resultant ySC3.1 and ySC4.1 strains were checked via PCR to determine if the repair fragment was integrated into the genome (**Supplementary information, Figure S1**). The RF3_fwd and RF3_rev primers were used to check the ySC3.1 strain and the RF4_fwd and RF4_rev primers were used to check the ySC4.1 strain (**Supplementary information, Table S3**). For both these strains the PCR was expected to yield a band of around 4000 bp if the construct was integrated into the genome (**Supplementary information, Figure 2**).

Table 1. Repair fragments produced in this study for construction of optogenetic Cln2 strains.

Repair fragment	Genotype	Location of insertion
RF3	X1(UP)-EL222(5xBS)-prSpo13-Kozak-Cln2-mNG-X1(DOWN)	X1
RF4	X1(UP)-GAL(UP)-EL222(5xBS)-prGAL1-Kozak-Cln2-mNG-X1(DOWN)	X1

Growth experiments with the Chi.Bio turbidostat

The turbidostat consisted of a control computer that was plugged into a laptop with which the turbidostat could be controlled. A reactor vessel was connected to this control computer and to a set of peristaltic pumps. These pumps would add fresh medium, remove excess culture and add the cells to the culture. The culture was grown in a glass vial of 20 mL and the OD was measured every minute. In between measurements the culture was stirred and activated with 500 nm light, if the experiment involved optogenetic activation (Steel *et al*., 2019).

To set up an experiment, the tubing was first flushed with 70% ethanol and then with sterile dH_2O because the salts from the medium and the ethanol might react and damage the tubing. The tubing was then filled with the medium or culture that was going to flow through it. The glass vials were autoclaved before use and kept in a sterile environment during assembly. 20 mL of fresh YPD medium and a stirring bean were added to the glass vial. The glass vial was then closed with a cap that allowed for attachment of the tubing. The stirring bean and cap were sterilized with 70% ethanol before use. The system was blanked by taking a measurement of the medium and this raw value was input as the zero point for the system. The cells were then added to the culture and the experiment was started. The system has a function to dither the OD, meaning that the cells are grown until they exceed 110% of the target OD and are then diluted to 90%. The cells are then allowed to grow again and this cycle can continue indefinitely as long as fresh medium is supplied. The system uses the data points to calculate a growth rate. This growth rate can be converted to a doubling time via the formula:

$$Doubling\ time\ (hours) = \frac{\ln(2)}{growth\ rate}$$

After the experiment was finished the tubing was flushed with sterile dH_2O and then with 70% ethanol to prevent biofilms growing on the inside and clogging the walls of the tubing. The turbidostats automatically calculated a growth rate from the OD measurements and produced a smoothed curve by taking a rolling average of the growth rate at each time point. However, the growth rate started at 2.0 by default, which corresponds to a doubling time of 21 minutes. The turbidostats required 1 to 2 hours to converge from a growth rate of 2.0 to the true growth rate. For this reason the first 2 hours of the experiment were discarded when calculating the growth rate of each strain. The remaining hours were averaged to calculate the growth rate in the period when the strains are growing at a constant rate.

To make calibration curves for the turbidostats, a culture of wild type YSBN6 was grown overnight in YPD and diluted to OD 0.1 the following morning. 20 mL of this diluted culture was then allowed to grow in one of three turbidostats. Every hour the culture was placed in each of the other two turbidostats and the OD value calculated by each turbidostat was recorded. As a control, the OD of the culture was also measured in the spectrophotometer every hour. The system was then tested with new targets to ensure that the actual ODs of the culture were 0.5. WT YSBN6 was grown overnight and then diluted to OD 0.5. The culture was allowed to grow in the turbidostats and the growth rate was calculated.

In the next calibration experiment, a YSBN6 culture was grown in YPD to an OD of 0.5 and then this culture was used to blank the three turbidostats. The system allows for blanking with solutions that do not represent an OD of 0 by measuring the current in the photodiode of the turbidostat and

manually inputting the OD that this current represents. The system then automatically calculated what measured current would correspond to OD 0 and sets this value as the blank value. These new blank values were used and a culture was grown with a target OD of 0.5 and the growth rates were measured.

During the experiments to calculate the growth rates of the strains, each strains was grown in duplo with a target OD of 0.5. The cells were grown overnight in a 10 mL culture of liquid YPD and diluted to OD 0.1 in the morning in 50 mL YPD. During these preculture steps, the flasks were covered with a jacket made from aluminium foil. When the culture had an OD of 0.5, 20 mL of culture was grown in YPD in each turbidostat. During the growth experiment with the flow cytometer, the cells were grown in a culture of 20 mL YPD at 30 ^{o}C and 300 rpm. Every hour 200 µL of the culture was put in the flow cytometer and the number of cells was counted in a sample of 20 µL. This measurement was used to calculate the number of cells per mL of culture. To grow strains in the dark, the flasks were covered with an aluminium foil jacket. To grow strains in the light, two rows of 4 blue LEDs were placed in the corner of the incubator and the flasks were placed in this corner of the incubator.

Data analysis

The microscopy images were analyzed with the BudJ annotation tool (Ferrezuelo *et al*., 2012). The images were manually annotated to record the budding of daughter cells. The time of birth of a daughter cell was defined as the time point at which a dark line appears in the bud neck between the mother and daughter cell. The G1 duration of the first cell cycle of the daughter cell was calculated as the difference between the time of birth and the time at which the first bud is produced by the daughter cell.

The volume of the cells was calculated with the YeaZ neural network (Dietler *et al*., 2020). The images were uploaded to a Jupyter notebook used to interface directly with the YeaZ program. The cells that were annotated with BudJ for the calculation of the G1 duration were used to determine the correlation between the volume of the cells and their G1 duration and time of birth. For each cell that was annotated in BudJ the location of the cell was found in the masks generated by the YeaZ program. The volume of the cell was then determined by summation of all the pixels in the mask.

To assess the number of dead or arrested cells, the images of each position on the slide after 400 minutes were visually inspected. If a cell was black with a light vacuole, this was considered a cell death. The next 20 time points were also visually inspected to see if any cells that were still alive were incapable of dividing. A cell death was considered to be the result of problems with budding if the cell had died while a bud was still attached to it. For each position the fraction of dead and arrested cells was calculated and the fractions were pooled for each position to yield the average fraction of dead or arrested cells in a given experiment.

Statistics

All statistical tests were performed in R 4.1.0 (R core team, 2021). The dplyr (version 1.0.6), car and ggplot2 packages were used for data analysis and visualization (Wickham *et al*., 2021; Fox & Weisber, 2019; Wickham, 2016). For comparing the means, the kruskall.test and pairwise.wilcox.test were used. For the pairwise Wilcoxon test, the Bonferroni p-adjustment was used. The lm and cor.test functions were used for linear regression and the spearman rank test, respectively. The cor.test used the spearman method.

Table 2. Strains used.

Strain	Genotype	Description
yAK31.2.1	cln2, cln3Δ, Whi5-mCherry, HO: prAct1-EL222(AQTrip)-CYC1	Parental strain containing EL222(AQTrip) for producing ySC3.1 and ySC4.1
yAK38.2.1	cln2, cln3Δ, Whi5-mCherry, HO: prAct1-EL222(AQTrip)-CYC1, CLN2: EL222(5xBS)-prSpo13-Kozak-Cln2-mNG	Optogenetic strain with EL222-controlled Cln2 in the endogenous CLN2 locus using the Spo13 promoter
ySC3.1	cln2, cln3Δ, Whi5-mCherry, HO: prAct1-EL222(AQTrip)-CYC1, X1: EL222(5xBS)-prSpo13-Kozak-Cln2-mNG	Optogenetic strain with EL222-controlled Cln2 in the X1 locus using the Spo13 promoter
ySC4.1	cln2, cln3Δ, Whi5-mCherry, HO: prAct1-EL222(AQTrip)-CYC1, X1: GAL(UAS)-EL222(5xBS)-prGAL1-Kozak-Cln2-mNG	Optogenetic strain with EL222-controlled Cln2 in the endogenous CLN2 locus using the GAL1 promoter
WT	YSBN6 wild type	Wild type control
cln2,3Δ	cln2, cln3Δ, Whi5-mCherry	cln2, cln3 double deletion control

Results

The EL222 construct

The optogenetic construct used for activation of Cln2 was a variant of the VP-EL222 system developed by Rullan *et al*. (2018). The system consists of a TF built from a nuclear localization signal (NLS), a VP16 trans-activation domain and the photosensitive EL222 protein. In response to blue light, the construct dimerizes and binds to the EL222 binding sequence on the DNA. In this active state, the protein stimulates transcription of any gene placed downstream of the binding sequence. In the inactive state the protein shows very little DNA binding activity and transcriptional activation. In this study, the AQTrip variant is used instead of the wild type EL222 protein. The AQTrip has a half-life of roughly 33 minutes whereas the WT variant has a half-life of 30 seconds (Zoltowski *et al*., 2013). This variant was chosen because the CFP laser of the microscope is used to activate the EL222 and this occurs once per five minutes when the cells are imaged. A 30 second half-life would mean that the EL222 is inactive during most of the experiment and therefore a stabilized variant was used.

Microscopy of optogenetic Cln2 in the endogenous locus

The previously constructed and yAK38.2.1 (**Table 2**) was characterized with single cell microscopy. This strain contained the optogenetic Cln2 construct in the endogenous CLN2 locus. The construct was placed in the endogenous locus to have a Cln2 expression in the light that is similar to that of WT. First, the strains were grown for 9 hours without any light stimulation to assess the G1 duration without any Cln2 expression. Next, the strains were grown for 9 hours with light stimulation to see the effect of Cln2 expression on the G1 duration. The WT and cln2,3Δ strains were used as controls to compare the phenotype of the optogenetic strain to. Moreover, this strain was characterized to determine the rate at which the EL222 AQTrip mutant reverses from the activated to the inactivated state and to determine whether the Spo13 promoter has sufficiently high expression levels to see the fluorescent signal from the mNeonGreen tag. To do this, the strains were grown for 3 hours in the light, followed by 6 hours in the dark, to see the reversal of the strain from the light phenotype to the dark phenotype. To assess the changes to the cell cycle by the optogenetic activation of Cln2 expression, the G1 duration of the daughter cells was calculated for each experiment based on the brightfield images. Specifically, the G1 duration of the daughter cells was calculated based on the time between the darkening of the bud neck and the production of the first bud by the daughter cell.

First, the yAK38.2.1 strain was imaged in the light and the dark to assess the effect of the optogenetic construct. Initial inspection of the fluorescent images revealed that the fluorescently tagged Cln2 was not expressed in sufficient numbers to be visible (**Figure S1**). The mean G1 duration of yAK38.2.1 when grown for 9 hours in the dark was 109 minutes (**Figure 1**). The cln2,3Δ strain had a mean G1 duration of 97 minutes, whereas the wild type had a mean G1 duration of 62 minutes. The resemblance of yAK38.2.1 to cln2,3Δ indicates that the yAK38.2.1 strain has little Cln2 expression in the dark. When the same strains were grown for 9 hours with light stimulation of EL222, yAK38.2.1 had a mean G1 duration of 44 minutes. The cln2,3Δ strain had a mean G1 duration of 90 minutes and the wild type strain had a mean G1 duration of 68 minutes (**Figure 1**). Here, the yAK38.2.1 strain resembles the WT strain more, which shows that Cln2 is produced in the light. The yAK38.2.1 actually has a shorter G1 duration than WT because the optogenetic systems bypasses the need for Cln3 to inhibit Whi5 before

Cln2 can be expressed.

Next, the yAK38.2.1 strain was grown for 3 hours in the light, followed by 6 hours of growth in the dark in order to determine how fast the optogenetic system shuts off after activation. The G1 duration of yAK38.2.1 was 40 minutes in the light and 48 minutes in the dark (**Figure 2**). This discrepancy between G1 duration when grown completely in the dark as opposed to when grown in the light before returning to the dark suggested that the optogenetically activated Cln2 stays activated after EL222 is no longer stimulated. It was hypothesized that this could be caused by other regulatory elements acting on the CLN2 locus, so the next strains were constructed to circumvent this. Alternatively, the slow reversal of the EL222 system could lead to the results lack of off-switching behaviour.

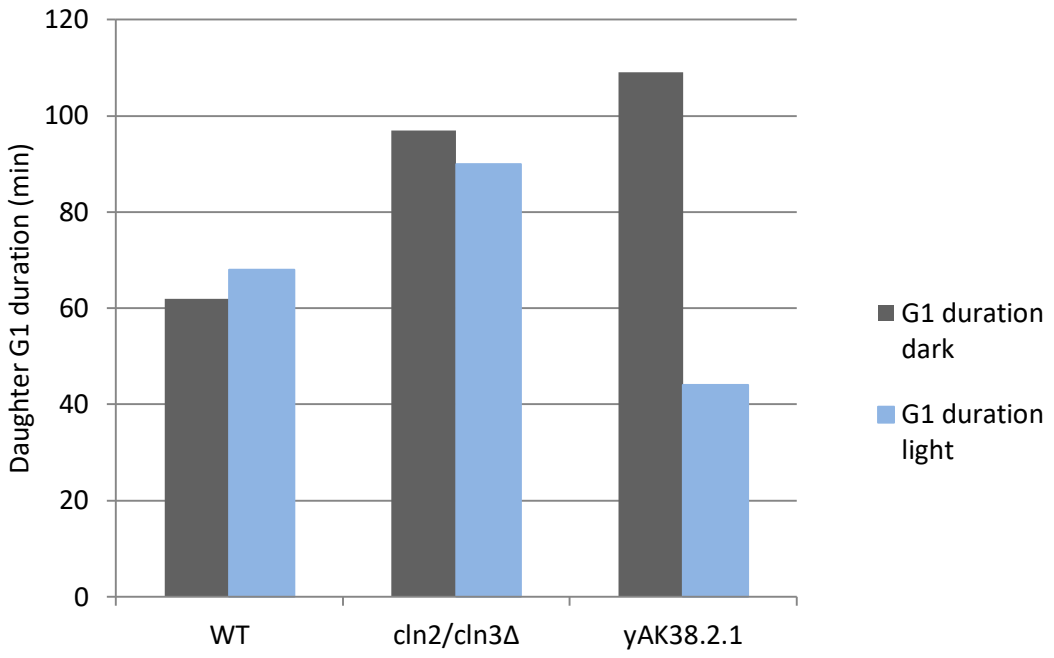

Figure 1. Mean G1 duration of yAK38.2.1 with Cln2 in endogenous locus and controls under constant lighting condition. The strains were grown for 9 hours under constant lighting conditions.

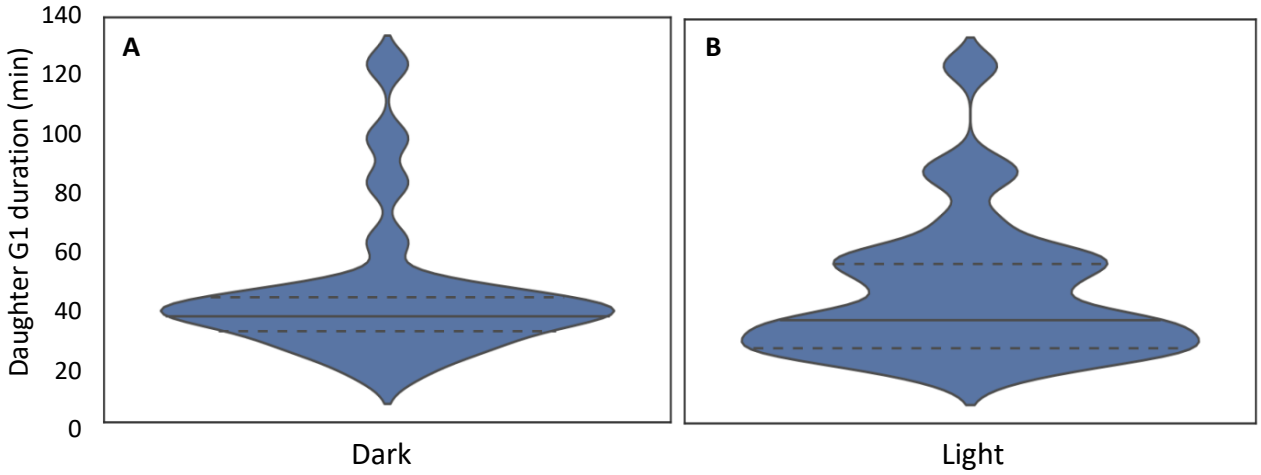

Figure 2. G1 duration of yAK38.2.1 in the light and after reverting to the dark. The solid lines represent the median G1 duration and dotted lines represent the 1st and 3rd quartiles. (A) Distribution of the G1 durations of daughter cells that were born in the first 3 hours. These cells were born while the light stimulation was active (B) Distribution of the G1 durations of the daughter cells that were born during the 6 hours after the light was turned off.

Phenotypes of optogenetic Cln2 strains under constant lighting conditions

To avoid any additional regulatory effects besides that of EL222, new strains were constructed with the optogenetically regulated Cln2 located in the X1 locus. The ySC3.1 strain was constructed with the weak Spo13 promoter and the ySC4.1 was constructed with the relatively strong Gal1 promoter. The new ySC3.1 and ySC4.1 strains were characterized with microscopy and by making growth curves in the turbidostat. The baseline G1 duration of the strains were determined based on microscopy experiments where the strains were grown entirely in the dark and in the light. The G1 duration of the WT and cln2,3Δ strains were similar to what was observed in the first experiments. The WT strain has a mean G1 duration of 58 minutes (s.d. = 21.6) whereas the cln2,3Δ strain has a mean G1 duration of 115 minutes (s.d. = 52.5). However, the experimental strains had lower G1 durations in both the light and the dark than the controls, which is different from the first experiments with Cln2 in the endogenous locus. The ySC3.1 and ySC4.1 strains have a similar distribution of G1 duration in the dark (**Figure 3**). The mean G1 duration of ySC3.1 is 45.9 (s.d. = 9.0) minutes and the mean G1 duration of ySC4.1 is 42.9 (s.d. = 15.1) minutes. However, in the light the G1 durations of the two strains diverge. The ySC4.1 strain has a higher mean (53.5 minutes; s.d. = 24.3 minutes) than the ySC3.1 strain (33.1 minutes; s.d. = 23.6 minutes), indicating that the weaker Spo13 promoter produces faster budding daughters than the stronger Gal1 promoter. This is an unexpected result, since the stronger promoter should produce more Cln2 and therefore reduce the G1 duration more. The G1 duration actually increased in the light for the ySC4.1 strain which is the opposite of the reported effect of Cln2 expression. The Cln2 expression in the ySC4.1 strain is possibly so high that it leads to detrimental effects for the cells, which could explain the increase in G1 duration in response to light. This would also explain why both strains had a shorter G1 duration in both light conditions than the WT strain. High leakage of the promoters could lead to enough Cln2 expression to trigger the positive feedback loop and push the cell past the START checkpoint. The

strain with the optogenetic construct in the endogenous locus does not show this, which indicates that the X1 locus is responsible for this behaviour.

A Kruskall-Wallis test was performed to calculate whether there was a difference in the mean G1 durations of the WT, cln2,3Δ, ySC3.1 and ySC4.1 strains in the dark and the light. The non-parametric Kruskall-Wallis test was used because the data violates the assumption of normality of an ANOVA (Kruskall & Wallis, 1952). The same Kruskall-Wallis test was used to test whether there was a difference in the volumes of these strains with and without light stimulation. A pairwise Wilcoxon rank sum test was used for post-hoc pairwise comparisons between groups (Fay & Proschan, 2010). A Bonferroni correction was applied to prevent false positives due to the use of multiple statistical tests (Bonferroni, 1936). The Kruskall-Wallis test shows that there is a significant difference between the mean G1 duration of at least one pair of categories ($p < 0.001$). The WT and cln2,3Δ strains had significantly different means ($p < 0.001$). The ySC3.1 and ySC4.1 had different means from each other ($p = 0.0023$) and different means from the WT and cln2,3Δ strains ($p < 0.001$ for all comparisons). The mean G1 duration of ySC3.1 was significantly lower in the light than in the dark ($p < 0.001$). The opposite was shown for the ySC4.1 strain, where the mean G1 duration is significantly higher in the light than in the dark ($p = 0.005$). The G1 duration of the ySC4.1 strain in the light was not significantly from the WT strain ($p = 0.532$).

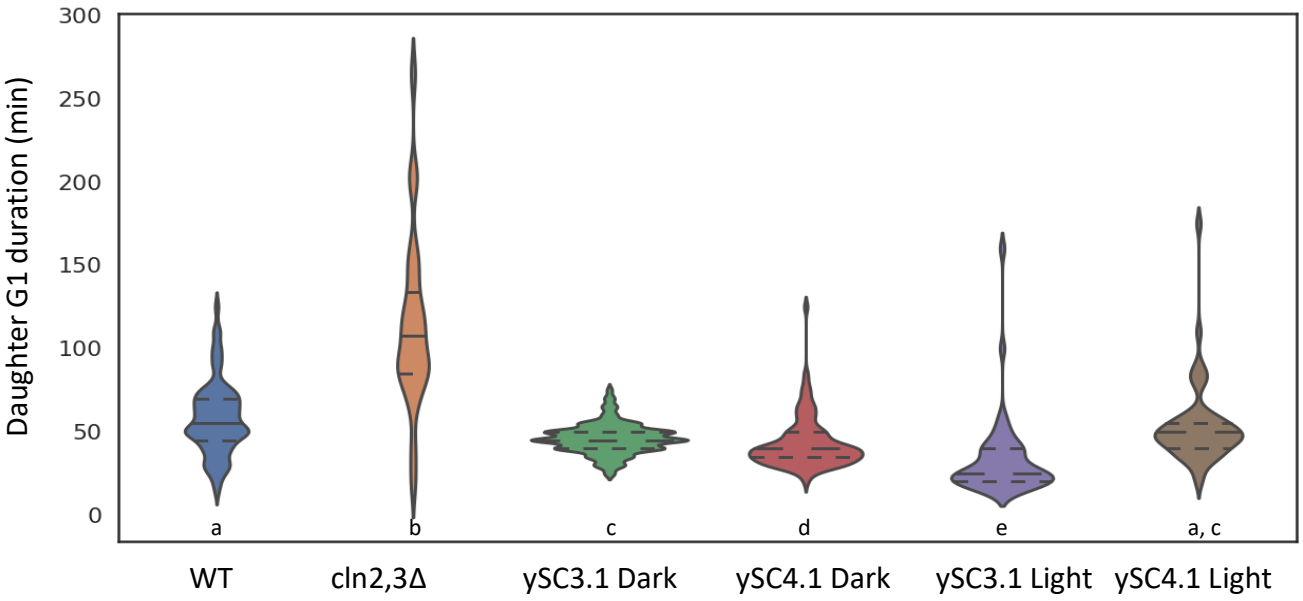

Figure 3. G1 durations of daughter cells from strain ySC3.1 and ySC4.1 in constant dark or light. The dark experiments consisted of 12 of growth without any optogenetic stimulation. The light experiments consisted of 12 hours of growth with 1% intensity CFP stimulation. Lines in the violins represent the 1st, 2nd and 3rd quartiles. Each letter corresponds to a group or several groups that have a non-significant difference between their means. Multiple letters indicate that a group has the same mean as two other groups that do have different means from each other.

The size of the cells was also assessed with the YeaZ neural network. Cln2 has an effect on average cell size as well as the cell cycle. Therefore, the effect of the optogenetic Cln2 construct should also be visible through changes in cell size in response to light. The same Kruskall-Wallis test and Wilcoxon

pairwise comparison that were used for the G1 duration were used with the cell volume data to test the significance of any observed differences. The controls show that deletion of Cln2 increases cell size. The WT has a significantly smaller size than all other strains ($p < 0.001$ for all comparisons), with an average cell size of 484 pixels (s.d. = 178) (**Figure 4**). The cln2,3Δ strain on the other hand, had a significantly larger size than all other strains ($p < 0.001$ for all comparisons), with an average cell size of 1299 pixels (s.d. = 425). Based in these observations, the size of the cells from the optogenetic strains was expected to decrease when the EL222 was activated compared to when the EL222 is inactive. When the cells are grown without light stimulation for 12 hours, the ySC3.1 cells have a mean volume of 1238 (s.d. = 401) pixels (**Figure 4**). The ySC4.1 cells have a mean volume of 1162 (s.d. = 320) pixels in the dark. There is no significant difference between the average cell size of ySC3.1 and ySC4.1 in the dark ($p = 1.0$). This indicates that both strains have a similar amount of Cln2 in the absence of light. Therefore, the promoters likely have roughly equal leakage. In the light ySC3.1 cells have a mean volume of 903 (s.d. = 350) pixels, whereas the ySC4.1 cells have a mean volume of 1117 (s.d. = 378) pixels. In the light, the difference between ySC3.1 and ySC4.1 does become significant ($p < 0.001$) The difference between average volume in the dark and in the light was significant for both ySC3.1 and ySC4.1 ($p < 0.001$ for both comparisons). The cells do become smaller in the light, which is in line with expectations, but they are still larger than the WT cells. This suggests that the optogenetic strains have Cln2 expression levels between WT and cln2,3Δ, whereas the G1 durations suggested them to have higher Cln2 expression than the WT. The difference could be explained by the fact that the G1 duration relies on the positive feedback loop instigated by Cln3. This leads to a delay in the WT strain but is not a factor in determining cell size. Another explanation is the observation that the buds from optogenetic strains stay attached to the mother cell longer than buds of the WT strain. Therefore, when the cells separate, the daughter cells of the ySC3.1 and ySC4.1 strains have a larger size than the WT daughter cells. The decrease in cell volume of ySC3.1 and ySC4.1 shows that Cln2 is expressed in higher levels in the light than in the dark. However, ySC4.1 was expected to show a larger decrease than ySC3.1 while the opposite is observed. This could again be due to the high expression levels of this promoter and the deleterious effects of Cln2 very high abundance. This result and the same unexpected behaviour of the G1 duration of ySC4.1, show that the strain is not performing as intended.

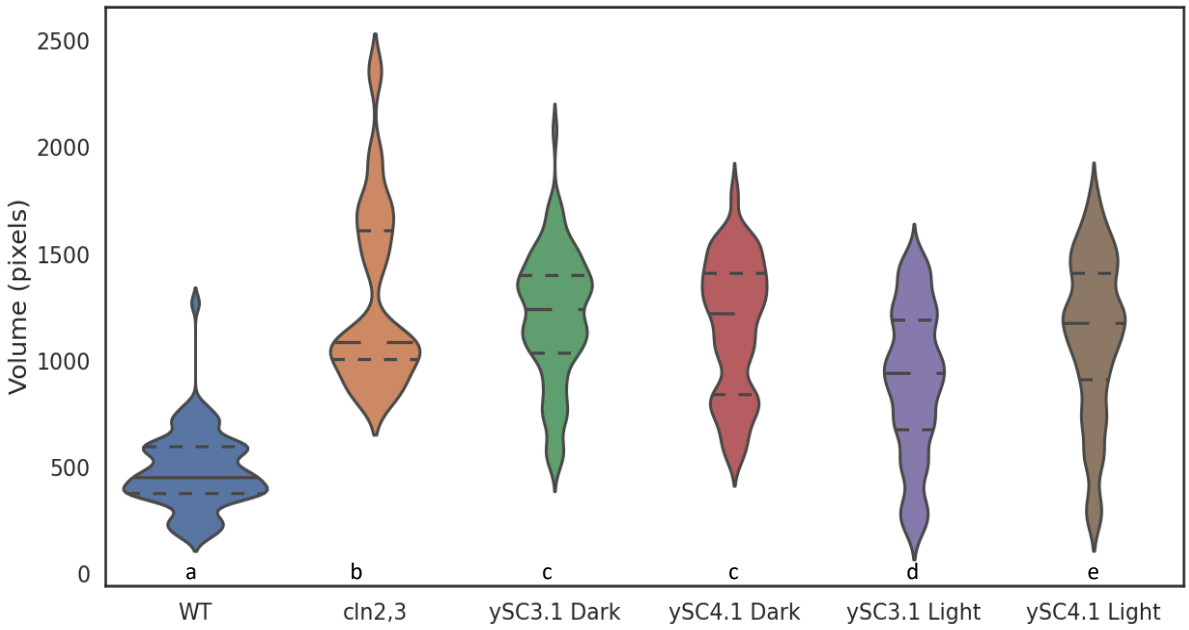

Figure 4. Volume distributions of ySC3.1 and ySC4.1 cells with and without light stimulation. The volume of the cells was calculated with the YeaZ neural network. The cells were grown for 12 hours with 1% CFP light stimulation of Cln2 expression. Lines in the violins represent the 1st, 2nd and 3rd quartiles. Each letter corresponds to a group or several groups that have a non-significant difference between their means.

Estimating growth rates of ySC3.1 and ySC4.1

To corroborate the changes in G1 duration of the ySC3.1 and ySC4.1 strains in response to light, their growth rates were calculated under different lighting conditions. It was expected that the shorter G1 duration of ySC3.1 in the light would be reflected in a shorter doubling time overall. Similarly, the increase in G1 duration of ySC4.1 in the light was expected to show up as a longer doubling time in the light. Assessing the growth rate of the constructed strains with flasks of culture that were sampled every half hour was labour-intensive and provides low resolution data. Therefore, a small turbidostat with a volume of 20 mL was used. The turbidostats were from Chi.Bio and could keep the temperature at a set point and shine 500 nm light on the culture to activate the EL222 (Steel *et al*., 2019). These turbidostats measured the OD of the culture every minute, which gives more detailed data with less effort than using a flask in the shaker. This set up allowed for up to four growth experiments to be carried out in parallel with minimal oversight. However, the turbidostats initially had large variability between different devices and needed to be calibrated before they could be used to gather reliable data.

First, the OD of a culture calculated separately by three turbidostats was compared with the OD measured by a validated spectrophotometer. The ODs calculated by the turbidostats all have a different slope and intercept but do follow a roughly linear pattern (**Figure 5**). The linearity of the data means that the doubling time can still be calculated accurately along a small OD range. However the non-zero intercept of the calibration curves can influence the data since it leads to a number of undetected cells that do not contribute to the measured OD but do contribute to the number of new cells created in a given timespan. This would bias the growth rate and make the measurements unreliable.

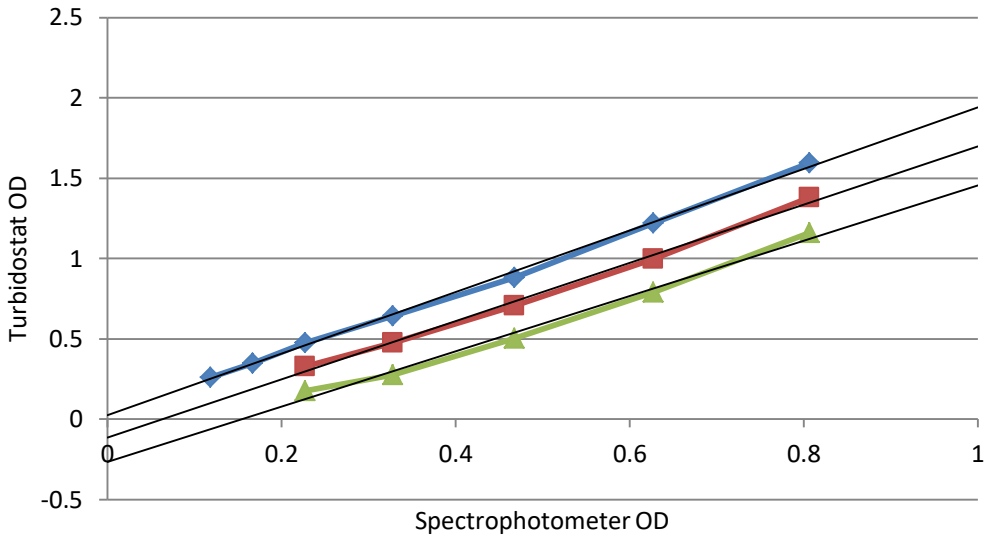

Figure 5. Calibration curves of OD measured by the different turbidostats compared to the OD measured by a spectrophotometer. OD measurements from a validated spectrophotometer are on the X-axis; OD measurements from the three turbidostats are on the Y-axis. A single culture was grown for 7 hours in the first turbidostat and the OD was measured every hour by all three turbidostats and the spectrophotometer. Blue: Turbidostat 1; Red: Turbidostat 2; Green: Turbidostat 3. During the first two hours no measurements were made with turbidostats 2 and 3.

Based on the calibration curves the targets were set to correspond to a real OD of 0.5. To test whether this setup yields accurate and consistent growth rates, WT YSBN6 was grown in three turbidostats with adjusted OD targets. Decreasing the variability of the system was more important than increasing the accuracy of the measurements. The OD targets were derived from the calibration curves to reflect OD 0.5 on the spectrophotometer. The growth curves are truncated to remove the first two hours, since the rolling average calculated by the turbidostat needs more than 100 time points to converge on the true growth rate. The growth rates lie between 0.36 and 0.53 $hour^{-1}$, with an average of 0.42 $hour^{-1}$ (**Figure 6A**). The average growth rate was close to the expectation if the system was properly calibrated but the growth rates show a lot of variation between turbidostats. During this experiment it was noticed that the current measured by the photodiode of the turbidostat was very similar between turbidostats when measuring the OD of cultures with an OD of 0.5 but very different when measuring the OD of fresh YPD medium for blanking. Based on this observation, it was hypothesized that the system might be influenced by ambient light during blanking and that the effect was less pronounced when measuring the OD of a dense culture. Next, the system was blanked with a culture of OD 0.5 and a WT culture was grown with an target OD of 0.5. The resulting growth curves were then used to see if the system could reliably reproduce the 90 minute doubling time of the WT YSBN6 strain. In this experiment, the growth rates were higher but less variable (**Figure 6B**). The average growth rate was 0.64 $hour^{-1}$, with the growth rates lying between 0.59 and 0.69 $hour^{-1}$. While these growth rates correspond to doubling times significantly faster than the 90 minutes characteristic of YSBN6, the growth rates are consistent. Since

this consistency is more important than reproducing the expected growth rate, the second calibration method was preferred and used for future experiments.

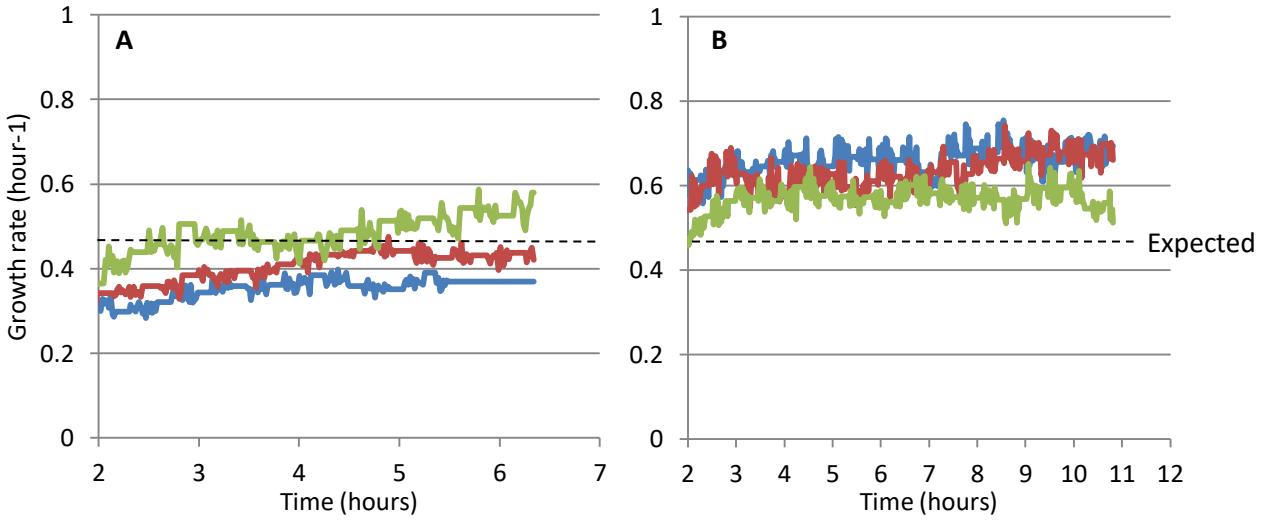

Figure 6. Growth rate of WT YSBN6 after calibration. The WT strains were grown under identical conditions in the three turbidostats. The expected growth rate of the strain was 0.46 hour^{-1}, corresponding to a doubling time of 90 minutes. This expectation is represented by the black dotted lines. Blue: Turbidostat 1; Red: Turbidostat 2; Green: Turbidostat 3. (A) Growth curves with adjusted OD targets; Turbidostat 1: 1.0, Turbidostat 2: 0.8, Turbidostat 3: 0.6. (B) Growth curves after blanking with a culture of OD 0.5 instead of YPD.

After the calibration, the growth rates of the optogenetic ySC3.1 and ySC4.1 strains were determined under different lighting conditions. The WT and cln2,3Δ strains were also grown as controls. To back up the findings from the turbidostat the strains were grown in flasks and the cell count was measured every hour with a flow cytometer. The flow cytometer can more accurately measure the number of cells in a culture, but it cannot be measured every minute. The strains were allowed to grow for seven hours and the doubling time of each strain was calculated from the cell counts. The growth rates from the turbidostat show that the wild type, with a growth rate of 0.624 hour^{-1}, grows faster than the optogenetic strains under most lighting conditions (**Figure 7**). The only exception is the ySC4.1 strain when grown in the dark. This is different from the G1 durations observed under the microscope, where the WT was slower than the optogenetic strains. However, under the microscope it was observed that daughter cells of the optogenetic strains stay attached to the mother cell longer before separating than WT daughter cells. The shorter G1 duration could therefore be compensated for by a longer G2 duration in ySC3.1 and ySC4.1 strains. This would explain why the decrease in G1 duration compared to the WT does not lead to a decrease in overall doubling time. Comparisons between lighting conditions for the optogenetic strains confirm the observations from the microscope. The growth rate of the ySC3.1 strain grows from 0.446 hour^{-1} in the dark to 0.532 hour^{-1} when grown in the light. The ySC4.1 strain shows the opposite trend. Its growth rate decreases from 0.624 hour^{-1} in the dark to 0.478 hour^{-1} in the light. While the difference between light and dark is the same as observed under the microscope for both strains, the growth rate of ySC3.1 and ySC4.1 in the dark is different. In contrast, the G1 durations of these

strains in the dark were similar. This indicates that the strains behave differently in a way that does not show up in the G1 duration data, though it is unclear what this behaviour could be. The cln2,3Δ strain grows much slower than any other strain, with a growth rate of 0.169 $hour^{-1}$. In contrast to the turbidostat, the data from the flow cytometer shows very little difference between the different optogenetic strains and different lighting conditions. It is unclear what causes these differences, but the data from the flow cytometer contains no replicates and is therefore less reliable. The growth rate experiments show that the observations from the microscopy experiments are largely confirmed by the data from the turbidostats, but not by the data from the flow cytometer.

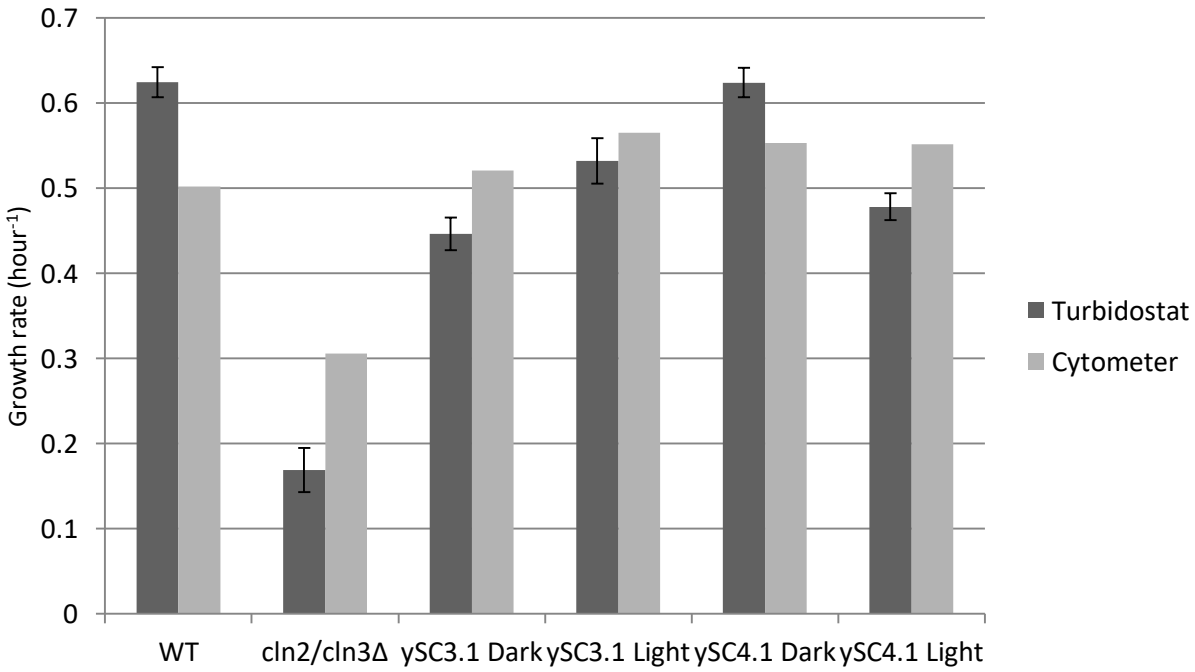

Figure 7. Growth rates calculated with data from the turbidostat and the flow cytometer. Error bars show 1 standard deviation. There were no replicates from the flow cytometer so this data has no standard deviation.

Phenotypical transitions in response to activation/deactivation of Cln2

Next, the dynamic properties of the EL222 regulated Cln2 systems were assessed. This was done by growing each strain for 4 hours in one lighting condition and then switching to the other lighting condition for 8 hours. First, the activation of the system was tested. If the system worked as expected based on previous observations, the daughter cells of the ySC3.1 and ySC4.1 strains should show a quick decrease in G1 duration when stimulated with light. To estimate the rate of activation of the optogenetic system, a linear regression was performed to calculate the correlation between the amount of time passed since the transition at time of birth and the G1 duration of the daughter cell. A linear regression was performed because inspection of the plots revealed no strong non-linearities in the data. The data was separated into data points before the transition and data points after the transition. The transition was set as timepoint 0 and the time of birth of the daughter cells was converted to the

number of hours after this transition. A linear regression was then performed on the data points after the transition to see whether there was a significant rate of increase or decrease in G1 duration as the cells transitioned from the activated state to the deactivated state or vice versa. The same type of linear regression was then performed with the volumes of the cells to determine whether there was a significant rate of increase or decrease in cell volume after the transition. In cases where the assumptions of a linear regression were violated a non-parametric Spearman rank correlation test was performed to determine whether there was any correlation between time of birth and volume or G1 duration (Wayne, 1990).

To assess the activation of the optogenetic construct, the cells were grown for 4 hours without any light and then grown for 8 hours with light stimulation. The daughter cells of the ySC3.1 strain have a mean G1 duration of 31.2 minutes (s.d. = 6.8 minutes) before any stimulation is applied (**Figure 7A**). After the EL222 is stimulated the G1 duration decreases slightly to 30.6 minutes and the variation increases to a standard deviation of 13.5 minutes. Despite the small magnitude of the decrease, it is strongly shown in the linear regression, which shows a decrease of -4.38 minutes per hour after light stimulation is applied ($p < 0.01$). This large slope is caused by a small increase in G1 duration right after the light switches on. The sudden expression of Cln2 could bring the cells out of equilibrium and lead to a transient increase in G1 duration around the switch. This would mean that the slope does not represent an actual decrease in G1 duration. However, the initial G1 duration of 31.2 minutes in the dark is much shorter than what was observed in the steady state experiments (45.9 minutes). Moreover, the G1 duration increases around the moment of the light switch before decreasing. The G1 duration calculated in the steady state experiments is the average of the cells born between 0 and 12 hours, while the G1 duration calculated here is the average of cells born between 0 and 4 hours. The G1 duration could possibly be influenced by factors such as crowding and competition for nutrients that increase with the time of birth. This would explain the changes in G1 duration between experiments but would also confound the relationship between time of birth and G1 duration in the transition experiment. If this is the case, the initial increase would be caused by other factors than the light stimulation but the decreasing trend after the light stimulation starts would represent a strong response of the optogenetic construct to the light.

The ySC4.1 starts with a much higher mean G1 duration (55.8 minutes; s.d. = 38.1 minutes). The mean G1 duration is 35.8 minutes (s.d. = 12.9 minutes) after the Cln2 expression is stimulated with light (**Figure 7B**). This what is expected from the optogenetic Cln2 construct, but the opposite of what was observed in the steady state experiment. However, this decrease already begins before the light is turned on. This is also reflected in the statistical analysis, which shows no significant correlation between G1 duration and the time passed since the light transition (correlation coefficient = 0.484 min/hour, $p = 0.62$). This indicates that the drop in G1 duration is not caused by the light stimulation. Also, the results here again contradict the findings from the steady state experiments, but the relationship between the time of birth and the G1 duration is not caused by the light switch. This indicates that there is an unknown factor that changes the G1 duration over time that is missed in the population averages of the steady state experiment. One possibility is that the cells are stressed by the transfer to the microscope slide and are still recovering in the beginning of the experiment.

The volumes of the daughter cells were also calculated from the masks found by the YeaZ neural network and compared with their time of birth and G1 duration. Since visual inspection indicated that

ySC3.1 and ySC4.1 daughter cells stayed attached to the mother cell for longer and this resulted in larger volumes at birth and shorter G1 durations, the correlation between cell volume and G1 duration was calculated. It was expected that the cells with a larger volume at birth would have a shorter G1 duration. However, there was no detectable correlation between the G1 duration of the cells and their volume for either strain (ySC3.1: $p = 0.946$; ySC4.1: $p = 0.452$) (**Supplementary Information, Figure 4A & 4B**). The correlation between the volume and the time of birth was calculated to see the effect of the light switch on the cell size. The average volume of the cells was expected to go down over time after the light is turned on and this was expected to coincide with a shorter G1 duration. Before the light is turned on, the ySC3.1 cells have an average volume of 779 pixels (s.d. = 363.5). After turning on the light, the volumes of the cells of ySC3.1 does not increase or decrease significantly as the time of birth increases. The volume data violated the assumption of heteroscedasticity so a Spearman-rank test was performed instead of a linear regression (rank correlation coefficient = 0.0147, $p = 0.8724$) (**Figure 8A**). However, the cell volume after the light is turned on is higher, averaging 831 pixels (s.d. = 283.8). These average volumes are similar to the volumes of ySC3.1 in the light during the steady state experiments. Combined with the anomalous results of the G1 duration, this indicates that some light pollution may have activated the EL222 and the cells are still partially activated when they are grown in the dark. The cells were only handled in a dark room with red lights, so any activation of the EL222 would be the result of very low amounts of light. The cells of ySC4.1 have a higher average volume than ySC3.1 before the light is turned on, with an average of 1286 pixels for ySC4.1 compared to 779 pixels for ySC3.1 (**Figure 8B**). The variation of ySC4.1 cells is lower than that of ySC3.1 cells; the standard deviation of ySC4.1 is 222 pixels. The volumes of ySC4.1 show a slight trend downwards after the light is turned on (-52.46 pixels per hour, $p < 0.01$). The results of ySC4.1 do align with the results observed in the steady state experiment. Together the data of the G1 duration and cell volumes indicate that ySC3.1 does get activated by light, whereas ySC4.1 does not respond to light.

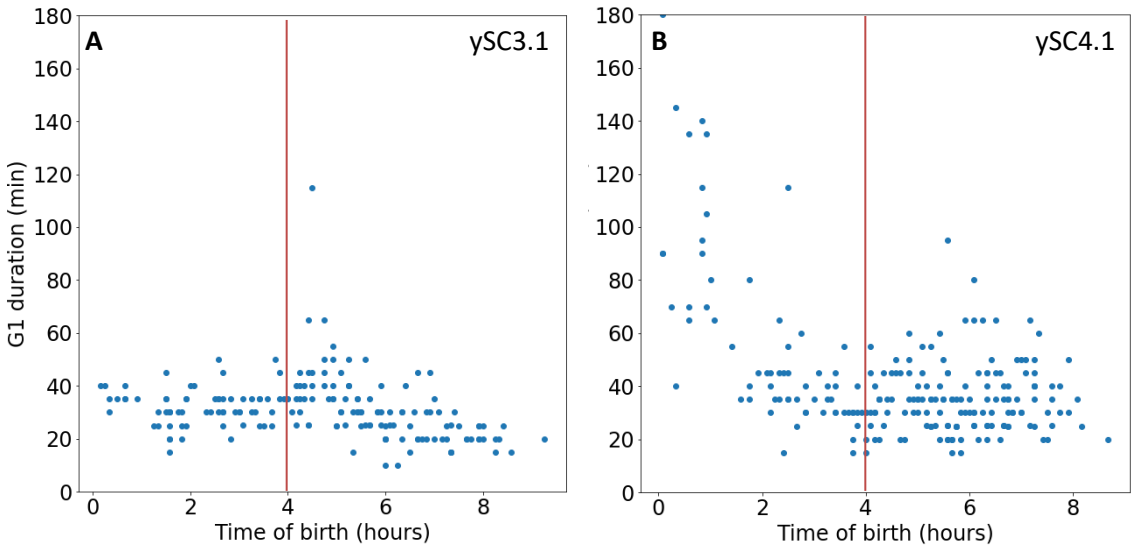

Figure 7. G1 duration as a function of time of birth of daughter cells of ySC3.1 and ySC4.1. The cells were grown in the dark for the first 4 hours of the experiment and received 1% CFP light stimulation for

the next 8 hours. (A) G1 durations of daughter cells of the ySC3.1 strain. (B) G1 durations of daughter cells of the ySC4.1 strain.

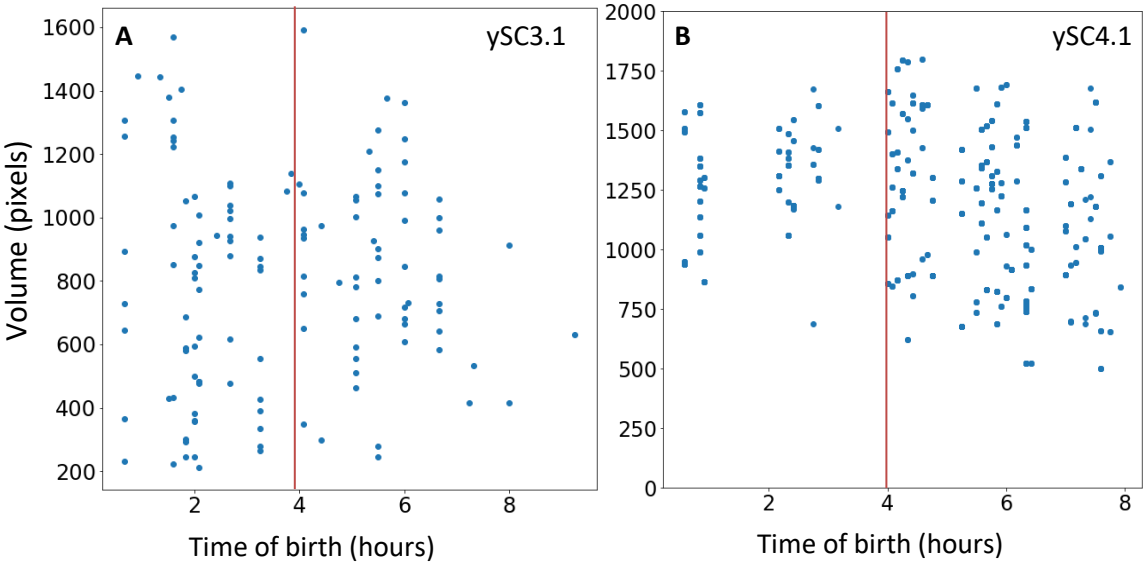

Figure 8. Volumes of daughter cells of ySC3.1 and ySC4.1 as a function of the time of birth. The cells were grown in the dark for the first 4 hours of the experiment and received 1% CFP light stimulation for the next 8 hours. Volumes were determined based on the masks generated by the YeaZ neural network. (A) Volumes of daughter cells of the ySC3.1 strain. (B) Volumes of daughter cells of the ySC4.1 strain.

After assessing the activation of the optogenetic Cln2 system, the inactivation of the system was characterized. To estimate the reversal time of the EL222 system, the opposite experiment was conducted. During these experiments, ySC3.1 and ySC4.1 were grown for 4 hours with light stimulation and then 8 hours without stimulation. The reversal time of the EL222 system could be estimated from the time it took the G1 duration to return from the short duration back to the longer duration after the CFP laser was turned off. The ySC3.1 strain shows a mean G1 duration of 25.4 minutes (s.d. = 9.1 minutes) while the EL222 is stimulated (**Figure 9A**). When the light is turned off the mean G1 duration increases to 36.9 minutes and the standard deviation also increases 23.2 minutes. In this experiment the ySC3.1 strain is again faster than what was observed in the steady state experiments. In both transition experiments the cells have an initial G1 duration that is around 10 minutes shorter than the G1 durations observed in the steady state experiments. This indicates that this effect is not specific to the light or dark state. This makes it more likely that crowding or competition for nutrients is responsible for the different G1 durations. If the G1 duration is always shorter at the start of an experiment, this would not show up in the average of the steady state experiments, but would lead to a discrepancy between the G1 duration observed in the first phase of the transition and the steady state average.

The ySC4.1 strain shows exactly the opposite trend (**Figure 9B**). Its mean G1 duration is initially much higher than that of ySC3.1 in the light, with a mean of 51.8 minutes and a standard deviation of 29.8 minutes. This mean is 39.3 minutes after the light is turned off and the standard deviation is 18.0

minutes. However, this decreasing trend is already visible before the light is turned off. While the average G1 durations in the light and in the dark are similar to those observed in the steady states, the observed decrease does not appear to be a response to the light. Moreover, the data from the light-to-dark transition is very similar to that of the dark-to-light transition. This again indicates that the ySC4.1 strain does not respond to the light stimulation. A spearman rank test was performed in the same way as done for the dark-to-light transition, to estimate the rate of deactivation. The spearman-rank test shows no significant correlation between the G1 duration and the time of birth after the end of light stimulation for either ySC3.1 ($\rho = 0.052$, $p = 0.5908$) or ySC4.1 ($\rho = -0.129$, $p = 0.0826$). This corroborates the finding that ySC4.1 does not respond to the light and indicates that ySC3.1 does not respond to the light either.

The volumes of the cells were again calculated with the YeaZ neural network to see how Cln2 expression changed the morphology of the cells. The volume was calculated as a function of the time of birth of the daughter cell and its G1 duration. The correlation between G1 duration and volume was again calculated to test the hypothesis that larger cells require less time to grow before budding and therefore have a shorter G1 duration. Because the data violated the assumption of heteroscedasticity, a non-parametric Spearman rank correlation test was used instead of a linear regression. The microscopy data again shows no significant correlation between the G1 duration of the cells of either ySC3.1 and ySC4.1, and the volume of the cells (**Supplementary Figure 5A & 5B**). For ySC3.1 the rank correlation coefficient is 0.0794 ($p = 0.6357$) and for ySC4.1 the rank correlation coefficient is -0.0845 ($p = 0.2542$). The relationship between the volume and time of birth was tested to see whether the optogenetic strains show deactivation based on an increase in cell size after the light is turned off. The mean volume of the ySC3.1 cells with the stimulation of Cln2 expression is (mean = 1053 pixels; s.d. = 348 pixels) (**Figure 10A**). After the light stimulation ends, there is no statistically significant trend in the volume of the cells with respect to the time of birth. The rank correlation coefficient between the volume of the cell and the time of birth of ySC3.1 cells is 0.0080 ($p = 0.9076$). The mean volume of the ySC4.1 cells is higher than that of ySC3.1 (1355 pixels; s.d. = 446 pixels) (**Figure 10B**). The Spearman-rank test does show a significant correlation between the volume of the ySC4.1 cells and their time of birth after the light was turned off. The rank correlation coefficient between volume of the cells and time of birth is -0.1764 ($p = 0.0166$). The lack of correlation between the volume and time of birth of ySC3.1 again indicates that the optogenetic construct does not deactivate after the light stimulation ends. The decrease of the volume of ySC4.1 is the opposite of what is observed in the steady state experiment and also the opposite of the behaviour of a functioning optogenetic Cln2 construct. Taken together, the G1 duration and cell size data indicate that neither ySC3.1 nor ySC4.1 deactivates after the light is turned off.

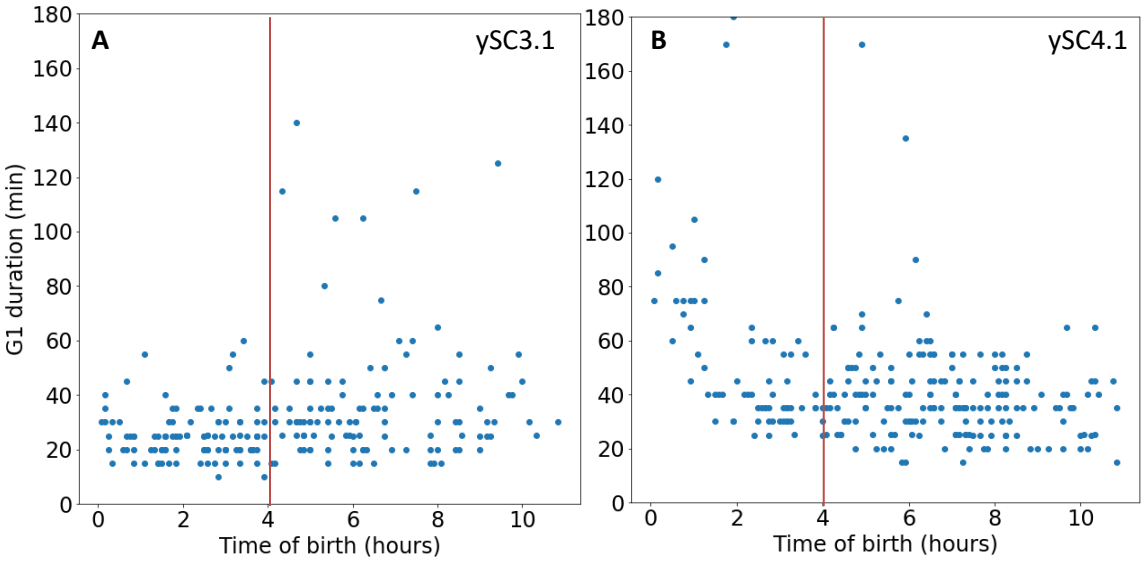

Figure 9. G1 duration as a function of time of birth of daughter cells of ySC3.1 and ySC4.1. The cells received 1% CFP stimulation for the first 4 hours of the experiment and no light stimulation for the next 8 hours. (A) G1 durations of daughter cells of the ySC3.1 strain. (B) G1 durations of daughter cells of the ySC4.1 strain.

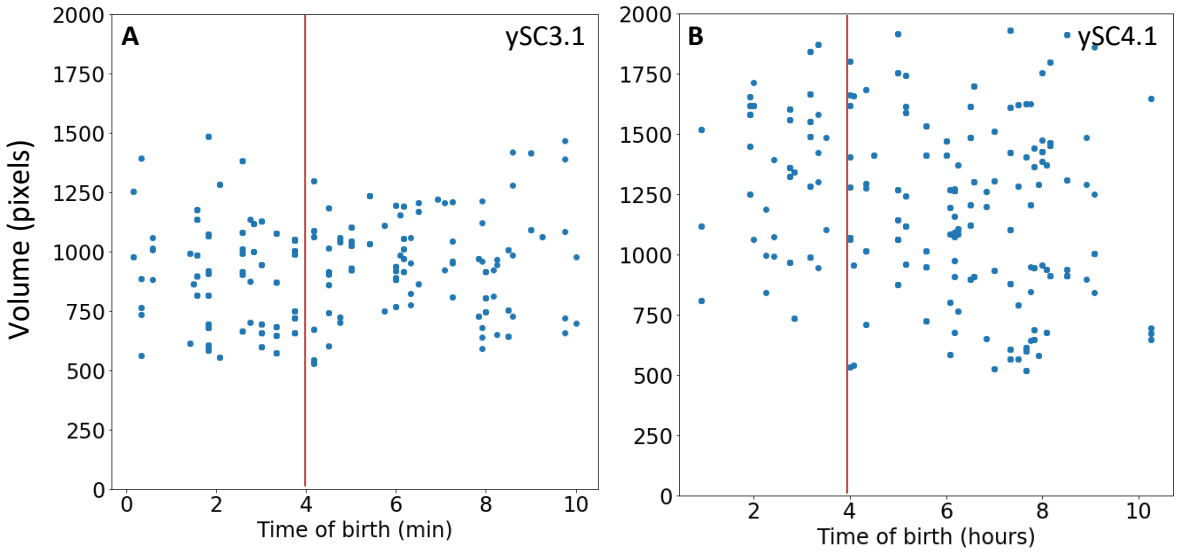

Figure 10. Volumes of daughter cells of ySC3.1 and ySC4.1 as a function of the time of birth. The cells received 1% CFP stimulation for the first 4 hours of the experiment and no light stimulation for the next 8 hours. Volumes were determined based on the masks generated by the YeaZ neural network. (A) Volumes of daughter cells of the ySC3.1 strain. (B) Volumes of daughter cells of the ySC4.1 strain.

In some experiments a large number of cells were observed to stop growing and dividing. Several cells were observed to grow a bud until it had attained the size of a full-grown cell, but the daughter cell never separated from the mother cell. To see whether this happens uniformly in all strains and under all conditions, in each microscopy experiment the fraction of cells that could no longer divide were counted

after 7.5 hours. This time point was chosen since the number of cells at later time points would grow to such an extent that manual counting of all cells was not feasible. The deaths and growth arrests were divided into those that happened while budding and those that happened while the cell was not budding. This was done because literature showed that Cln2 perturbation leads to trouble budding and also premature aging and cell death (Neurohr *et al*., 2018). It was expected that trouble budding would show up as deaths while budding, while premature aging would show up as deaths outside of budding. However, no consistent difference was seen in the prevalence of failures to bud and spontaneous cell death, indicating that there is one process responsible for increased cell death in the Cln2 mutant strains. A Kruskall-Wallis test and post-hoc Wilcoxon pairwise comparisons were used to test the significance of the difference of the fractions of dead and growth arrested cells for each strain and lighting condition. The non-parametric tests were used because the data violates the assumption of normality. The WT strain showed no deaths or growth arrest in any image (**Figure 11**). ySC3.1 also showed no growth arrest when grown in the dark but showed significantly more deaths and growth arrest in the light, both spontaneously and as a result of failure to bud ($p < 0.001$). ySC4.1 has the same rate of death and growth arrest as ySC3.1 in the dark ($p = 1.0$). In the light, the ySC4.1 has a significantly higher fraction of cells that die or stop growing than in the dark ($p = 0.028$). This indicates that light activation increases cell death and growth arrest. The ySC3.1 strain in the dark-to-light transition has a fraction of dead or arrested cells that is not statistically significant from neither the WT control, nor the ySC3.1 strain grown under the dark and light conditions. The ySC4.1 strain in the dark-to-light transition has significantly more cases of death and growth arrest than ySC4.1 grown in constant darkness ($p < 0.001$). The ySC3.1 strain in the light-to-dark transition also has a significantly higher fraction of dead or arrested cells than ySC3.1 grown in constant darkness ($p < 0.001$). The ySC4.1 strain in the light-to-dark transition has a significantly higher rate of death than the ySC4.1 grown in constant darkness ($p = 0.001$). The fraction of dead and arrested cln2,3Δ cells higher than that of WT ($p = 0.032$). The overall trend seen here is that the optogenetic strains have the largest fraction of dead and arrested cells when there is light activation during the experiment. The optogenetic strains in the dark, which have the lowest Cln2 expression, also have the lowest amount of dead and arrested cells. This seems to indicate again that the constructed strains have high Cln2 expression under all lighting conditions and that this coincides with high rates of death and growth arrest. However, the cln2,3Δ strain with no Cln2 expression also suffers from high rates of death and growth arrest. The data from this study indicates that both under- and overexpression of Cln2 can also lead to problems with bud formation and mitosis.

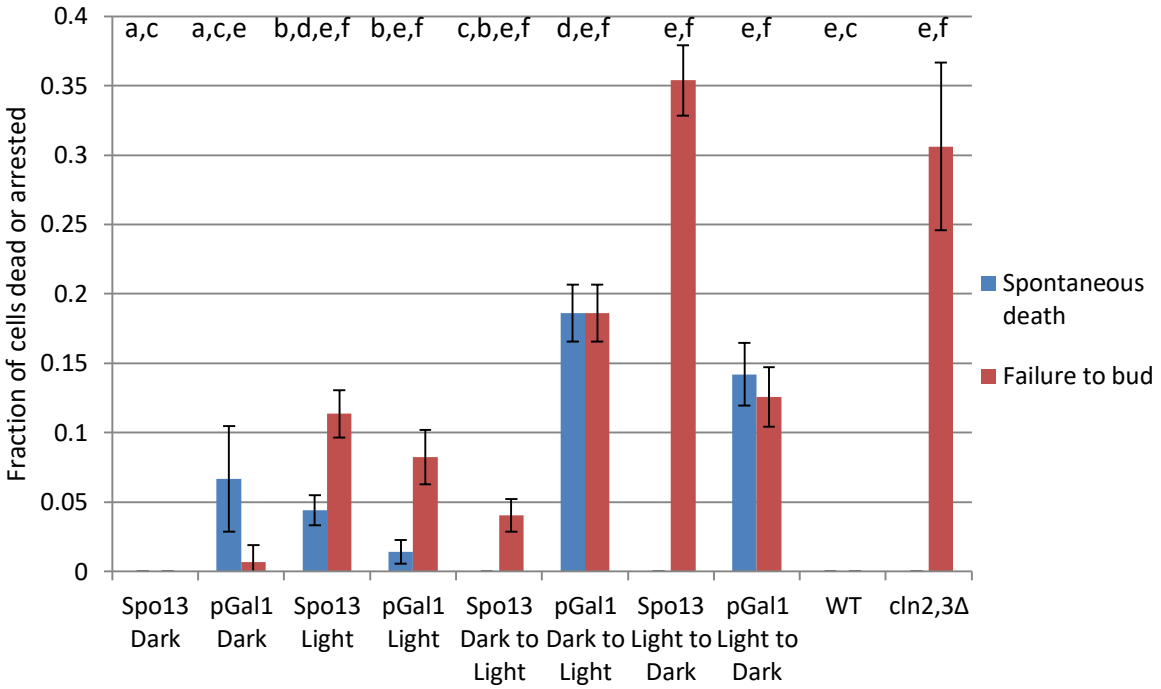

Figure 11. Fraction of cells that suffered from death or growth arrest. Deaths & growth arrests were divided based on whether the cell was producing a bud or not. Dead and arrested cells were counted after 7.5 hours. Error bars show one standard deviation. Each letter corresponds to a group or several groups that have a non-significant difference between their means. Multiple letters indicate that a group has the same mean as two other groups that do have different means from each other.

Discussion

The aim of this study was to build strains with optogenetic Cln2 that could be used to manipulate the cell cycle with the help of targeted light stimulation. Data was gathered from multiple sources and analyzed with advanced computational tools to provide a comprehensive characterization of these strains. The first strain tested, which lacked Cln3 and contained an optogenetically activated Cln2 in the endogenous Cln2 locus (yAK38.2.1), showed a clear reduction in G1 duration when Cln2 was transcribed versus when it was not being produced in the cell (**Figure 1**). This is explained by the general role of Cln2 as a G1/S cyclin, since actively producing Cln2 in response to light stimulation forces the cell past the START checkpoint. In WT, Cln3 first has to be transcribed to activate the positive feedback loop but the optogenetic system bypasses this and rapidly starts the transcription of Cln2 at full strength when the EL222 is activated. This explains why the optogenetic strains can have a shorter G1 duration in the light than the WT strain. However, the optogenetic strain did not revert to the cln2,3Δ phenotype when light stimulation ceased. This was initially thought to be caused by regulatory elements besides EL222 that could be acting on the CLN2 locus. For this reason the endogenous locus was abandoned in favour of the X1 locus which is well characterized and has no unknown regulatory elements acting on it.

The new constructed strains with the optogenetic Cln2 construct in the X1 showed a different behaviour from the yAK38.2.1 strain with Cln2 placed in the endogenous locus. Instead of showing the

double mutant phenotype, without light activation both the ySC3.1 and ySC4.1 strains had a shorter G1 duration than WT (**Figure 3**). This is likely due to leakage of the promoters in the X1 locus, which generates enough basal Cln2 production to trigger the feedback loop that leads to cell division. In the steady state experiments, ySC3.1 and ySC4.1 both had the same G1 duration of 40-45 minutes in the dark, which indicates that the leakage rate the Spo13 promoter and Gal1 promoter in the X1 locus are roughly equal. In the presence of light stimulation the two strains show divergent behaviour. The G1 duration of the ySC3.1 strain becomes shorter whereas that of the ySC4.1 strain becomes longer. This is likely due to the different strength of the promoters. The Spo13 promoter of the ySC3.1 strain has significantly lower expression levels than the Gal1 promoter of the ySC4.1 strain (Benzinger & Khammash, 2018). Combined with the increase in expression levels from the X1 locus, the ySC3.1 strain produces enough Cln2 to speed up the progression through START. In the ySC4.1 strain however, Cln2 is overproduced which leads to deleterious effects on the growth of the cells. It has been reported that overexpression of Cln2 leads to elongated cells, indicating that overexpression can lead to abnormal morphologies (McCusker *et al*., 2007). This type of deregulation of growth could be responsible for the increased G1 duration of the ySC4.1 strain when Cln2 expression is stimulated. This relationship between overexpression and elongated growth could also explain why the volume of the ySC3.1 cells decreases more in response to light than that of the ySC4.1 cells (**Figure 4**). The Gal1 promoter of the ySC4.1 cells could increase Cln2 expression to such high levels that growth abnormalities occur, while the expression levels of the Spo13 promoter do not reach high enough levels to cause this type of cell morphology.

The difference between ySC3.1 and yAK38.2.1 shows that the position in the X1 locus leads to a generally higher expression, since the constructs are the same and only the locus in which they are placed differs between the strains. This higher expression in the X1 locus than in the endogenous CLN2 locus could be caused by the chromatin being looser in the X1 locus than in the CLN2 locus. Because of these high expression levels in the X1 locus, the ySC3.1 and ySC4.1 strains are only capable of expressing Cln2 with relatively high abundances. This incomplete range of Cln2 abundance levels limits the extent to which the cell cycle can be influenced and further experiments should investigate Cln2 at these lower abundance levels. To attain lower levels of Cln2 production, the construct could be moved back into the endogenous locus since the lack of inactivation after stimulation is also present in the X1 locus. Instead, the lack of inactivation could be caused by the long reversal time of the AQTrip EL222 mutant. If a low level of active EL222 is still enough to cause sufficient Cln2 expression to trigger START, this would lead to the lack of deactivation observed in this study. This could be solved by replacing the current EL222 variant that has a half-life of 30 minutes with a shorter-lived EL222 variant. Alternatively, the presence of Cln1 could trigger a positive feedback loop that keeps the cells in the 'ON' state. To combat this, Cln1 could also be deleted from the genome. Deleting Cln1, Cln2 and Cln3 simultaneously is not possible, but in the current strains Cln2 is reintroduced (Edgington & Futcher, 2001). This makes it possible to remove Cln1 as well, although this would produce a strain that can only be grown in the presence of blue light. Besides changing the EL222 variant and removing Cln1, the construct could be altered to have lower expression levels. The current constructs have five EL222 binding sites and this number could be reduced in order to have lower expression levels of Cln2. The Kozak sequence in the ySC3.1 strain could also be removed to reduce the translation efficiency of Cln2 and thereby reduce levels of Cln2 in the strain. Since prSpo13 is already a very weak promoter, changing the promoter to an even weaker one is

likely not a good strategy. It will be very hard to find a promoter that is well characterized and has lower expression levels than prSpo13. Therefore, removal of several EL222 binding sites or the Kozak sequence would be the optimal way to reduce the expression of Cln2 in the construct.

The transition experiments showed several results that contradicted the results of the steady state experiments. The G1 duration of the ySC3.1 strain in the initial dark or light phase was 10 minutes faster than G1 duration in the corresponding steady state experiment. Since this occurs in both lighting conditions, it is unlikely that the light is responsible. Rather, it is most likely that there is some factor that changes during the course of the experiment. This would not show up in the average of the steady state experiment but would alter the average G1 duration if only the first 4 hours are taken into consideration. A possible factor would be crowding and competition for nutrients among the cells as the colonies grow. This would make it more difficult for cells to divide as the colony grows larger and lead to a longer G1 duration later in the experiment. For the ySC4.1 strain, the exact opposite was observed. The initial G1 duration was much higher than that observed in the steady state experiments. This was again observed for both transitions and the drop happens before the changing of the lighting condition, indicating that the lighting was not responsible. The G1 duration rapidly drops after the start of the experiment, which suggests that the source of stress does not come from the growth under the microscope, but rather something experienced beforehand. However, the exact source of the stress cannot be found from the data gathered in this study. To understand what is happening in these experiments, the strains should be grown under constant lighting conditions and the G1 duration should be plotted as a function of the time of birth. If these changes in G1 duration remain, it shows that there is some factor in the microscopy procedure that shifts the G1 duration. Further experiments could then pinpoint the responsible factor in an effort to eliminate it and resolve these anomalous observations.

While the transition experiments conflict with the steady state experiments, the growth rates calculated from the turbidostats generally support the findings of the steady state experiments. The effect of light on the doubling time of the ySC3.1 and ySC4.1 strains was the same as the effect on the G1 duration. However, the growth rates of the WT, ySC3.1 and ySC4.1 strain in the dark did not follow the G1 data from the steady state experiments. This variability could be due to the use of YPD medium, which is a complex medium and its contents are therefore not precisely known. Different batches of YPD could have slightly different compositions which could lead to differences in growth rate. This source of variation could be excluded by growing the yeast cultures in a synthetic medium such as YNB. Alternatively, the difference between WT and the optogenetic strains could be due to the fact that the ySC3.1 and ySC4.1 daughter cells stay attached to the mother longer and separate with a larger average cell volume. Recent work has found that the concentration of Whi5 decreases with increasing cell size (Schmoller *et al*., 2015). This would mean that less Cln2 is needed to clear Whi5 from the nucleus and trigger START. This could be confirmed by calculating the doubling time in the microscopy experiments as well. If a shorter G1 duration is caused by longer growth as a bud, the overall doubling time should be less affected by the optogenetic Cln2 expression than the G1 duration. One caveat is that the flow cytometer did not reproduce the trends observed in the turbidostats (**Figure 6**). The growth rates of the optogenetic strains were not different between strains or lighting conditions. While the data from the flow cytometer, comes from a single culture per strain and lighting condition, this does raise doubts about the validity of the turbidostat experiments. More experiments with both the turbidostats and flow cytometer would need to be performed to create a clearer picture of the relationship between light

conditions and growth rate of the optogenetic strains.

The cell size data in the steady state experiments show some response to the light but do not fully align with the observations of the G1 duration and doubling times. Based on the experiments with the microscope and turbidostats, it was expected that the cell size of the optogenetic strains was similar to that of the WT strain. However, the optogenetic strains in the dark had average cell volumes close to that of the cln2,3Δ strain. The cell volumes decreased in the light for both strains, but the volume of ySC3.1 decreased more than that of ySC4.1. If the large cell volumes were caused by a lack of Cln2 it would be expected that the stronger Gal1 promoter of ySC4.1 would lead to a bigger decrease than the Spo13 promoter of ySC3.1. An explanation could be that high levels of Cln2 expression lead to increased cell size. In fact, overexpression of Cln2 has been reported to lead to elongated cell growth (McCusker *et al*., 2007). Whereas the steady state experiments show a response to light, the transition experiments show no consistent respond to the light in either optogenetic strain. ySC4.1 shows a decrease in cell size after both transitions, so that is not caused by the light. This lack of any visible trend could be caused by the high variability of cell volumes calculated by the YeaZ neural network. Small trends could become lost in the noise. Moreover, the cell sizes calculated by YeaZ had more variation than visual inspection of the images would suggest. This could possibly be improved by including better error detection protocols in the YeaZ implementation. Currently, only implausibly small cells (smaller than 250 pixels) are filtered out during post-processing. The smallest WT cells were more than 250 pixels and many segmentation masks of this size are vacuoles of cells instead of whole cells. On the opposite end, the largest segmentation masks are often produced when the neural network misidentifies two cells that are close together as one cell. In this research, no criteria were found that could be used to throw away erroneous segmentations while retaining proper segmentations. This would be an avenue for further research that could improve the cell size analysis and possibly uncover small responses to changing lighting conditions.

Lastly, the results from the cell death and growth arrest experiments pose a problem for studying the cell cycle with these strains. If the large amounts cells from the optogenetic strains die in response to light, this impedes the study of these strains. Moreover, if the death rate is not equal for all cells in the population, it could bias research towards certain subpopulations of cells. For this reason, further research should attempt to determine what causes increased cell death and growth arrest and to resolve this issue during further strain construction. A trend that emerged is that the strains grown in constant light or in the transition experiments have a higher rate of death and growth arrest than the strains grown in the dark or the WT strain. A lack of Cln2 has been reported to lead to premature cell death (Neurohr *et al*., 2018). Cln2 has also been linked to the production of the septin ring in the bud neck and the delivery of vesicles to buds during growth (Gladfelter *et al*., 2005; Egelhofer *et al*., 2008; Moffat & Andrews, 2004). This could explain why cells with altered Cln2 levels have trouble producing buds and completing mitosis when they do.

While the strains constructed in this study do not have a cell cycle that responds to light input, although the range of phenotypes achievable with this system is does not fully span from the cln2,3Δ mutant with no Cln2 expression to the wild type levels of Cln2 expression. Further work could build on the insights from this work to create a strain with tunable Cln2 expression that spans the full physiological range. Successful construction of such a strain would pave the way towards a deeper understanding of cell cycle dynamics and full synchronization of a yeast culture. This could possibly be

realized with the turbidostats used in this research. These are fully programmable and a controller algorithm could be developed for synchronizing a culture. Recent efforts have shown that reinforcement learning algorithms are capable of keeping cell populations in a desired state in bioreactors (Treloar *et al*., 2020). These algorithms capable of learning are especially useful when the input data is highly complex and simple heuristics are insufficient to make predictions or generate desired outcomes, such as in biological systems (Francois-Lavet *et al*., 2018). While these applications are still far away, this work has made some progression towards the creation of a fully controllable optogenetic Cln2 strain.

Supplementary information

Protocols

PCR amplification of Gibson assembly parts

Amplification of all parts was done with a PCR using the Q5 DNA polymerase. The components of the PCR reaction are listed in **Table S1**. The temperatures and durations of each phase of the PCR is listed in **Table S2**. The primers used for the construction of the strains are listed in **Table S3**.

Table S1. Components for one PCR amplification

Component	Concentration	Volume per sample (µL)
Q5 Reaction buffer	5X	10
High GC enhancer	5X	10
Forward primer	10 µM	2.5
Reverse primer	10 µM	2.5
Q5 DNA polymerase	2000 U/mL	0.5
dNTPs	100 mM each	1
Template DNA	-	1
MQ H_2O	-	22.5

Table S2. Thermocycler program for the PCR using the Q5 polymerase

Step	Temperature (°C)	Duration (minutes:seconds)
Initial denaturation	**95**	**0:30**
Denaturation	**95**	**0:10**
Annealing	**Varies by primer**	**0:30**
Extension	**72**	**0:30 per kb**
Repeat	**-**	**34 times**
Final extension	**72**	**2:00**
Storage	**4**	**Indefinitely**

Table S3. List of primers used to construct strains.

Primer name	Sequence	Description
pFA6_fwd	AAGTTGAGTCGAGAATAATTAGAGGC GGTTTGCGTATTG	Primers for pFA6-GAL1(UP)-EL222(5xBS)-prGAL1-Kozak-Cln2-mNG
pFA6_rev	TACAATCTGCTCTGATGCC	Primers for pFA6-GAL1(UP)-EL222(5xBS)-prGAL1-Kozak-Cln2-mNG
GAL-UAS_fwd	CGGCATCAGAGCAGATTGTAGAATTT TCAAAAATTCTTACTTTTTTTTTG	Primers for pFA6-GAL1(UP)-EL222(5xBS)-prGAL1-Kozak-Cln2-mNG
GAL-UAS_rev	GAGGCTAGCGAAGATCTCCCACTTCA ATATAGCAATGAGC	Primers for pFA6-GAL1(UP)-EL222(5xBS)-prGAL1-Kozak-Cln2-mNG
EL222_fwd	GAGGACGCACGGCTCTAGTGTCTAAG	Primers for pFA6-GAL1(UP)-EL222(5xBS)-prGAL1-

	CTTCATGGACTAAAGGC	Kozak-Cln2-mNG
EL222_rev	ATATTGAAGTGGGAGATCTTCGCTAG CCTC	Primers for pFA6-GAL1(UP)-EL222(5xBS)-prGAL1-Kozak-Cln2-mNG
prGAL1_fwd	GACACTAGAGCCGTGCGTCCTCGTCTT C	Primers for pFA6-GAL1(UP)-EL222(5xBS)-prGAL1-Kozak-Cln2-mNG
prGAL1_rev	GCCATTTTGTTTTAATTAATATAGTTTT TTCTCCTTGACGTTAAAGTATAGAGG	Primers for pFA6-GAL1(UP)-EL222(5xBS)-prGAL1-Kozak-Cln2-mNG
Cln2-fwd	CTATATTAATTAAAACAAAATGGCTAG TGCTGAACCAAG	Primers for pFA6-GAL1(UP)-EL222(5xBS)-prGAL1-Kozak-Cln2-mNG
mNG_rev	CCAATACGCAAACCGCCTCTTTACTTG TACAGCTCGTCCATGCC	Primers for pFA6-GAL1(UP)-EL222(5xBS)-prGAL1-Kozak-Cln2-mNG
GAL1_Seq	TTAACTATGCGGCATCAGAG	Primer for sequencing pFA6-GAL1(UP)-EL222(5xBS)-prGAL1-Kozak-Cln2-mNG
Backbone_fwd	ATTAATTAAAACAAAATGGCTAGTG	Primers for second round of Gibson assembly for pFA6-GAL1(UP)-EL222(5xBS)-prGAL1-Kozak-Cln2-mNG
Backbone_rev	AAGATCTCCCACTTCAATATGCAATGA GC	Primers for second round of Gibson assembly for pFA6-GAL1(UP)-EL222(5xBS)-prGAL1-Kozak-Cln2-mNG
RF3_fwd	CCTGTTGCAATACTATACTACGTCTTG ACATGAACTCTCAACAGTGAAGCTTG GGAGATCTTCG	Primer for making repair fragment of EL222(5xBS)-prSpo13-Kozak-Cln2-mNG to integrate into X1 locus
RF3_rev	GAATACGGAGCCGTTTGTCTTTTACTG CGGGATTAACTTCAACATTACTTGTAC AGCTCGTCCATGC	Primer for making repair fragment of EL222(5xBS)-prSpo13-Kozak-Cln2-mNG to integrate into X1 locus
RF4_fwd	CCTGTTGCAATACTATACTACGTCTTG ACATGAACTCTCAACAGTGAATTTTCA AAAATTCTTACTTTTTTTTTGG	Primer for making repair fragment of GAL1(UP)-EL222(5xBS)-prGAL1-Kozak-Cln2-mNG to integrate into X1 locus
RF4_rev	GAATACGGAGCCGTTTGTCTTTTACTG CGGGATTAACTTCAACATTACTTGTAC AGCTCGTCCATG	Primer for making repair fragment of GAL1(UP)-EL222(5xBS)-prGAL1-Kozak-Cln2-mNG to integrate into X1 locus

Gibson assembly

The parts were assembled using a Gibson assembly with a premade Gibson Assembly mix. The volumes of each part of the Gibson assembly was calculated with the online Gibson assembly tool from New England Biolabs. All parts had an equivalent number of moles in the Gibson assembly reaction, with the exception of the EL222 part, which was 5 times more abundant than the other parts due to its small size. The first Gibson assembly was performed according to **Table S4**. After the components were mixed, the reaction mixture was incubated at 50 ^{o}C for 1 hour and then stored at 4 ^{o}C until use. Afterwards, competent DH5α cells were transformed with the assembled plasmid. The cells were grown and the plasmid was extracted for further use. After sequencing showed that the first Gibson assembly had only assembled three out of the five parts a new Gibson assembly with the partially assembled plasmid and remaining two components was designed (**Table S5**)

Table S4. Parts and concentrations of the Gibson assembly with five components

Component	Stock concentration (ng/uL)	Amount of product (pmol)	Volume (uL)
pFA6	130	0.064	0.77
Gal(UP)	52	0.064	0.62
EL222	35.4	0.321	1.21 (5-fold excess)
prGAL1	66	0.064	0.6
Cln2-mNG	263	0.064	0.41
MQ H2O	-	-	1.38
GA Mastermix	2X	-	5

Table S5. Parts and concentrations of the Gibson assembly with five components

Component	Stock concentration (ng/uL)	Amount of product (pmol)	Volume (uL)
pFA6-Gal(UP)-Cln2-mNG	181	0.064	1.27
EL222	118	0.321	0.67 (5-fold excess)
prGAL1	80	0.064	0.69
MQ H2O	-	-	2.37
GA Mastermix	2X	-	5

Transformation of DH5α

DH5α *E. coli* cells were made highly competent with Inoue buffer. The cells were grown overnight on a plate at 37 °C. Then a single colony was used to inoculate 25 mL LB and this culture was grown at 37 °C until the culture had reached OD 0.5. Then the culture was diluted 20 times and grown again until it had reached OD 0.5. The culture was then diluted in 50 mL SOB medium and grown at 18 °C until the OD was 0.5. The dilution was calculated so that the OD would reach 0.5 after 18 hours based on a doubling time of 280 minutes. The cells were then placed on ice-water for 10 minutes. Afterwards the cells were centrifuged for 10 minutes at 2500g and 1 °C. The cells were then washed with 25 mL Inoue buffer (**Table S6**). The cells were centrifuged again for 10 minutes at 2500g and 1 °C and resuspended in 4 mL Inoue buffer + 300 µL DMSO. The competent cells were then divided into aliquots of 50 µL and frozen at -80 °C until use. Upon use the cells were thawed and 5 µL of assembled plasmid was added. The cells were then incubated for 30 minutes in ice. The cells were then heat shocked at 42 °C for 30 seconds. The cells were then placed on ice again for 2 minutes and afterwards 950 µL LB medium was added. The cells were then incubated at 37 °C and 220 rpm for 1 hour and subsequently plated on selective LB agar plates. The plates were then incubated for 1 day at 37 °C. After the colonies had grown, single colonies were then grown overnight in 3 mL liquid LB with appropriate antibiotics at 37 °C. The liquid cultures were then miniprepped with a plasmid extraction kit (Macherey-Nagel) according to the protocols of the kit.

Table S6. Inoue buffer

Component	Concentration (M)
$MnCl_2$▪$4H_2O$	0.055
$CaCl_2$▪$2H_2O$	0.015
KCl	0.25
PIPES (pH 6.7)	0.01

CRISPR transformation of yeast

For each modification of a yeast strain the strain was transformed with a CRISPR plasmid containing the Cas9 protein, one or two sgRNAs and a resistance marker against the antibiotic nourseothricin, and a repair fragment containing the cassette that is inserted into the target locus. The parental strain was inoculated in 3 mL YPD and grown overnight at 30 ^{o}C and 300 rpm. The next day, the culture was diluted in 20 mL YPD to an OD_{600} of 0.2. The culture was grown for four hours to an OD_{600} of 0.9 to ensure that the cells were in the exponential growth phase. The culture was then diluted to OD_{600} 0.7 and 20 mL of this culture was pelleted for 3 minutes at 4000 rpm. The supernatant was discarded and the pellet washed with 25 mL sterile dH_2O. The pellet was then resuspended in 1 mL 0.1 M LiAc and transferred to a 2 mL tube. The cells were then spun down at 5000g for 2 minutes and resuspended in 320 µL 0.1 M LiAc. The cells were then aliquoted as 100 µL per transformation. The cells were spun down again at 5000g for 2 minutes and the transformation mix was added (**Table S7**). The ssDNA was boiled at 95 ^{o}C for 5 minutes and cooled on ice before adding it to the cells. The cells were vortexed and incubated at 42 ^{o}C for 40 minutes in a water bath. Afterwards, the cells were spun down for 2 minutes at 5000g and the supernatant was removed. The cells were resuspended in 1 mL YPD and incubated at 30 ^{o}C and 300 rpm for 2 hours. The cells were then spun down again at 5000g for 2 minutes and resuspended in 150 µL sterile dH_2O. The cells were then plated on YPD plates containing 50 µg/mL nourseothricin and incubated at 30 ^{o}C for 2 days.

Table S7. Transformation mix components and volumes.

Component	Amount
50% PEG 3350	240 µL
1 M LiAc	36 µL
ssDNA	25 µL
CRISPR plasmid	500 ng
Repair fragment	5 µg
Sterile dH_2O	Total volume up to 351 µL

Figures

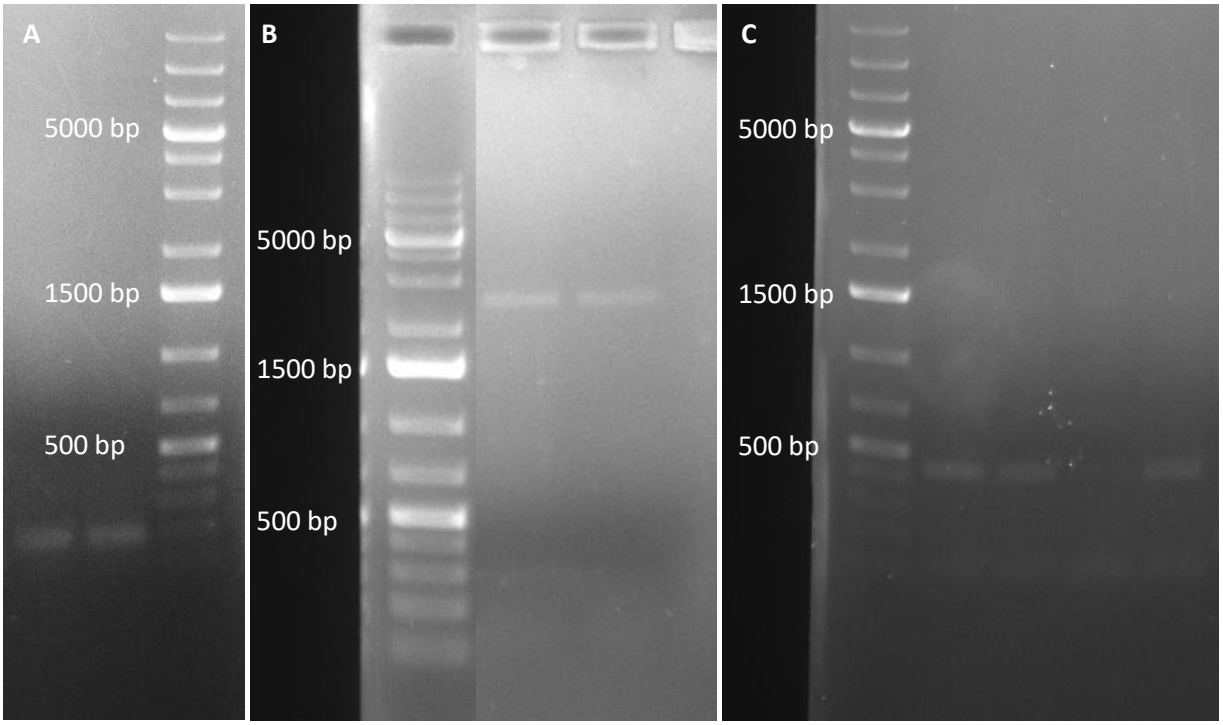

Figure S1. Gel images of PCR products of Gibson assembly parts. (A) PCR product of EL222. The expected band size was 291 bp. (B) PCR product of cln2-mNG. The expected band size was 2391. (C) PCR product of prGAL1. Expected band size was 431 bp.

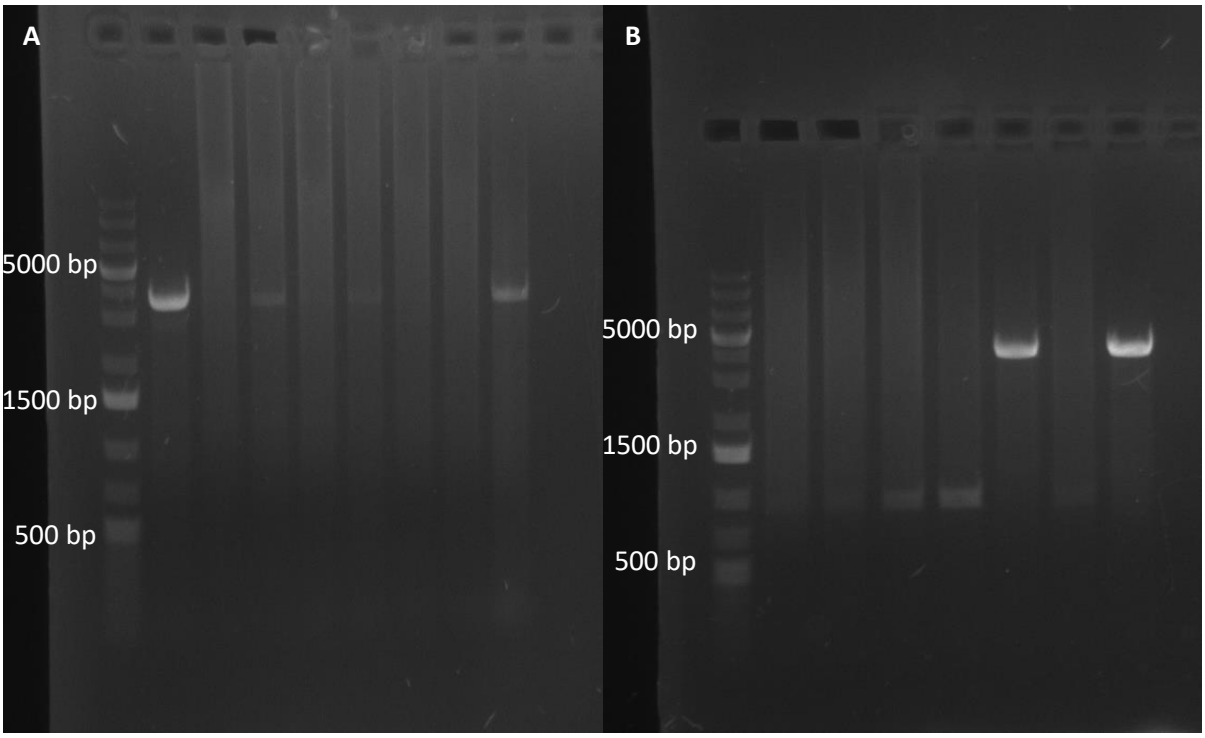

Figure S2. PCR verification of ySC3.1 and ySC4.1. Expected bands if insertion of the repair fragment into the X1 locus was successful are ~4000 bp. (A) Eight colonies of ySC3.1. (B) Eight colonies of ySC4.1.

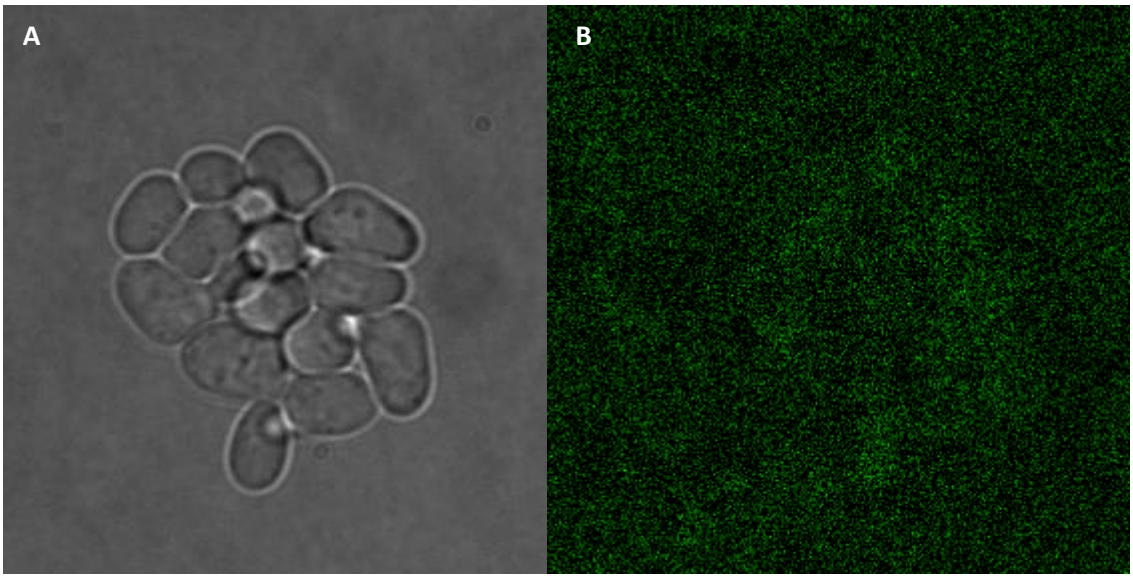

Figure S3. Fluorescent signal of Cln2-mNG in the endogenous CLN2 locus after optogenetic stimulation. The background was subtracted using the ImageJ function using a rolling ball radius of 50 pixels.

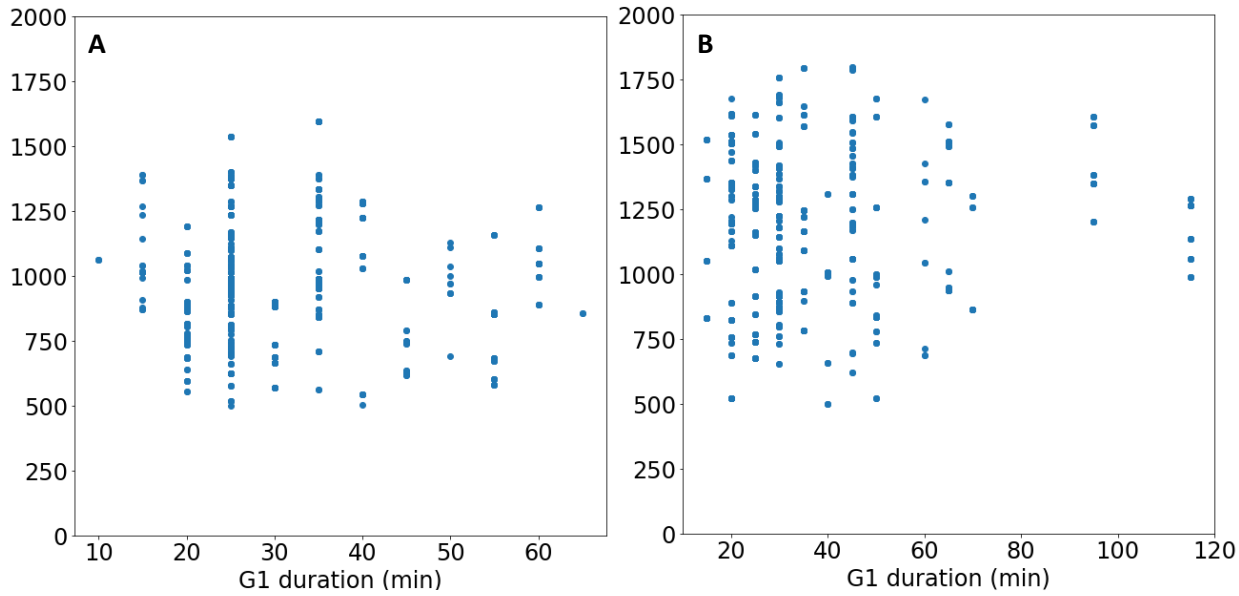

Figure S4. Correlation between G1 duration and cell volume in the transition from dark-to-light. For each daughter cell the G1 duration and volume was calculated during the transition experiments. (A) Relationship between volume and G1 duration of ySC3.1. (B) Relationship between volume and G1 duration of ySC4.1.

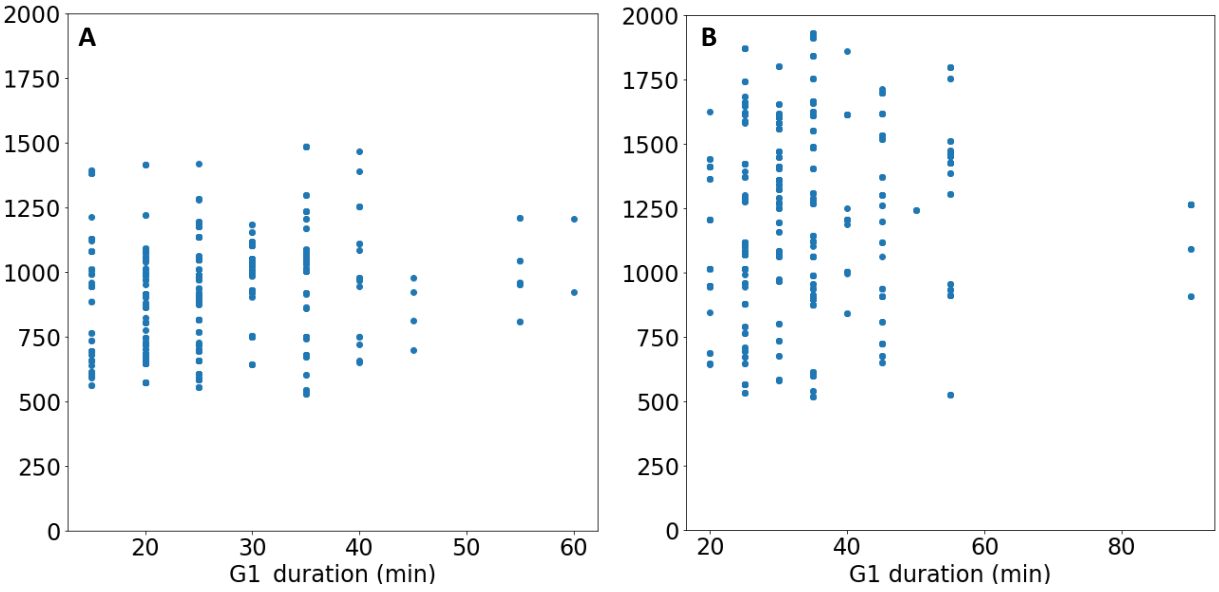

Figure S5. Correlation between G1 duration and cell volume in the transition from light-to-dark. For each daughter cell the G1 duration and volume was calculated during the transition experiments. (A) Relationship between volume and G1 duration of ySC3.1. (B) Relationship between volume and G1 duration of ySC4.1.

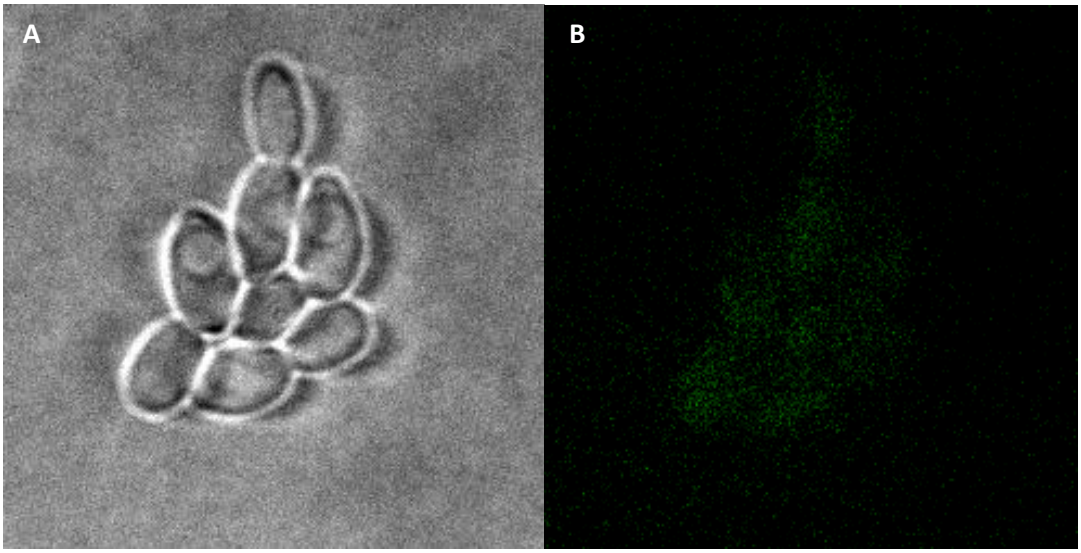

Figure S6. Fluorescent signal of Cln2-mNG in the X1 locus under control of the Spo13 promoter after optogenetic stimulation. The background was subtracted using the ImageJ function using a rolling ball radius of 50 pixels.

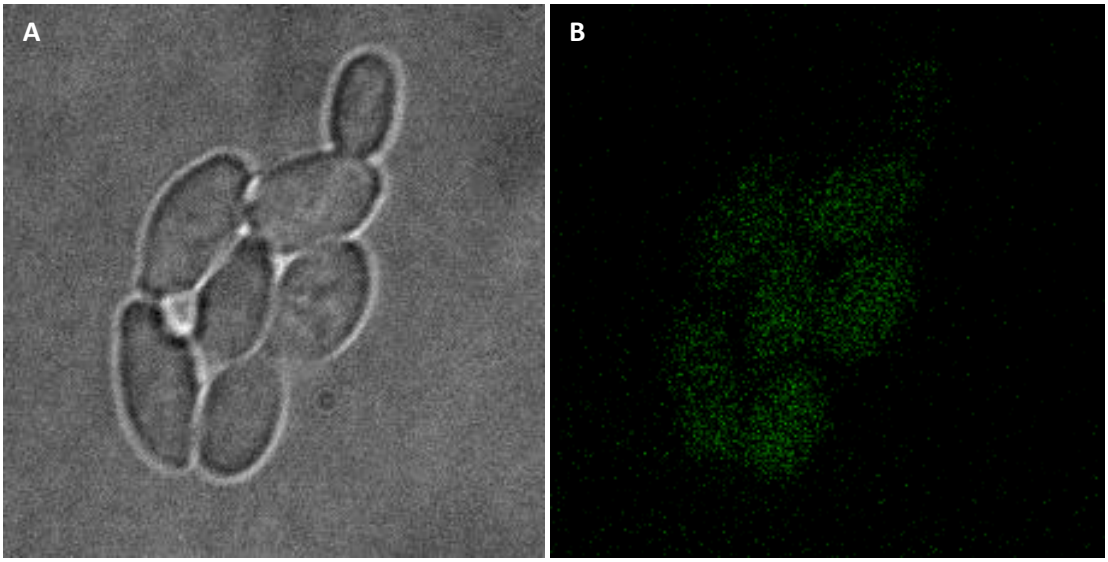

Figure S7. Fluorescent signal of Cln2-mNG in the X1 locus under control of the Gal1 promoter after optogenetic stimulation. The background was subtracted using the ImageJ function using a rolling ball radius of 50 pixels.

Sequences

Sequence 1. Sequence of pFA6-GAL(UP)-EL222(2xBS)-Cln2-mNG. The sequence contains the Gal(UP) part, 2 EL222 binding sites and the first several hundred bases of Cln2. The sequence of Cln2-mNG was already verified.

GCAATTCAAATTCTTACTTTTTTTTTGGATGGACGCAAAGAAGTTTAATAATCATATTACATGGCATTACCACCATAT
ACATATCCATATCTAATCTTACTTATATGTTGTGGAAATGTAAAGAGCCCCATTATCTTAGCCTAAAAAAACCTTCTC
TTTGGAACTTTCAGTAATACGCTTAACTGCTCATTGCTATATTGAAGTGGGAGATCTTCGCTAGCCTCGAGTAGGTA
GCCTTTAGTCCATGCGTTATAGGTAGCCTTTAGTCCATGAAGCTTAGACACTAGAGCCGTGCGTCCTCGTCTTCTAT
ACTTTAACGTCAAGGAGAAAAAACTATATTAATTAAAACAAAATGGCTAGTGCTGAACCAAGACCCCGTATGGGA
CTCGTCATCAATGCTAAACCGGACTACTATCCGATTGAGCTATCTAATGCAGAATTACTTTCTCACTTCGAAATGCT
GCAAGAATACCACCAAGAAATCTCCACCAATGTTATTGCTCAATCATGTAAGTTCAAACCTAATCCAAAACTAATAG
ACCAGCAGCCTGAAATGAACCCCGTGGAAACAAGGTCCAACATTATCACTTTTTTGTTCGAGCTGTCTGTGGTCAC
TCGAGTGACAAATGGTATTTTTTTTCATTCAGTTAGATTATATGACCGCTATTGTTCCAAGAGAATCGTGTTACGGG
ACCAAGCCAAATTGGTTGTCGCTACTTGTCTCTGGTTGGCTGCTAAAACTTGGGGCGGTTGTAATCACATCATCAAT
AATGTAGTCATCCCTACTGGCGGAAGATTTTATGGTCCCAACCCAAGGGCACGTATACCTCGACTCTCTGAACTAG
TTCATTACTGTGGTGATGGTCAGGTCTTTGATGAATCAATGTTTTTACAAATGGAAAGACATATACTAGACACTTTA
AATTGGAACATTTATGAACCAATGATCAATGATTACGTTTTAAATGTTGATGAAAATTGTTTGATGCAATACGAACT
TTATGAAAATCAAGTTACTTATGACAAACAATGCTCTGAAAAACGTCAGTCTCAATTATCCCAGGATAGTGATGCC
ACTGTAGACGAGAGGCCCTACCAAACGAAGAAGAGA

Sequence 2. Sequence of pFA6-GAL(UP)-EL222(5xBS)-prGAL1-Cln2-mNG. The sequence contains the GAL(UP), EL222 and prGAL1 parts and the first several hundred bases of Cln2. The sequence of Cln2-mNG was already verified

AAGAAATTCAAATTCTTACTTTTTTTTTGGGATGGGACGCAAAGAAGTTTAATAATCATATTACATGGCATTACCAC
CATATACATATCCATATCTAATCTTACTTATATGTTGTGGAAATGTAAAGAGCCCCATTATCTTAGCCTAAAAAAACC
TTCTCTTTGGAACTTTCAGTAATACGCTTAACTGCTCATTGCTATATTGAAGTGGGAGATCTTCGCTAGCCTCGAGT
AGGTAGCCTTTAGTCCATGCGTTATAGGTAGCCTTTAGTCCATGCGTTATAGGTAGCCTTTAGTCCATGCGTTATAG
GTAGCCTTTAGTCCATGCGTTATAGGTAGCCTTTAGTCCATGAAGCTTAGACACTAGAGCCGTGCGTCCTCGTCTTC
ACCGGTCGCGTTCCTGAAACGCAGATGTGCCTCGCGCCGCACTGCTCCGAACAATAAAGATTCTACAATACTAGCT
TTTATGGTTATGAAGAGGAAAAATTGGCAGTAACCTGGCCCCACAAACCTTCAAATTAACGAATCAAATTAACAAC
CATAGGATGATAATGCGATTAGTTTTTTAGCCTTATTTCTGGGGTAATTAATCAGCGAAGCGATGATTTTTGATCTA
TTAACAGATATATAAATGGAAAAGCTGCATAACCACTTTAACTAATACTTTCAACATTTTCAGTTTGTATTACTTCTT
ATTCAAATGTCATAAAAGTATCAACAAAAAATTGTTAATATACCTCTATACTTTAACGTCAAGGAGAAAAAACTATA
TTAATTAAAACAAAATGGCTAGTGCTGAACCAAGACCCCGTATGGGACTCGTCATCAATGCTAAACCGGACTACTA
TCCGATTGAGCTATCTAATGCAGAATTACTTTCTCACTTCGAAATGCTGCAAGAATACCACCAAGAAATCTCCACCA
ATGTTATTGCTCAATCATGTAAGTTCAAACCTAATCCAAAACTAATAGACCAGCAGCCTGAAATGAACCCCGTGGA
AACAAGGTCCAACATTATCACTTTTTTGTTCGAGCTGTCTGTGGTCAT

References

- Bean, J. M., Siggia, E. D., & Cross, F. R. (2006). Coherence and timing of cell cycle start examined at single-cell resolution. *Molecular cell*, *21*(1), 3–14. https://doi.org/10.1016/j.molcel.2005.10.035
- Benzinger, D., Khammash, M. Pulsatile inputs achieve tunable attenuation of gene expression variability and graded multi-gene regulation. *Nat Commun* **9,** 3521 (2018). https://doi.org/10.1038/s41467-018-05882-2
- Bertoli, C., Skotheim, J. M., & De Bruin, R. A. M. (2013). Control of cell cycle transcription during G1 and S phases. *Nature Reviews Molecular Cell Biology*, *14*(8), 518–528. https://doi.org/10.1038/nrm3629
- Bonferroni, C. E. (1936). Teoria statistica delle classi e calcolo delle probabilità, *Pubblicazioni del R Istituto Superiore di Scienze Economiche e Commerciali di Firenze.*
- Charvin, G., Cross, F. R., & Siggia, E. D. (2009). Forced periodic expression of G $_1$ cyclins phase-locks the budding yeast cell cycle. *Proceedings of the National Academy of Sciences*, *106*(16), 6632–6637. https://doi.org/10.1073/pnas.0809227106
- Costanzo, M., Nishikawa, J. L., Tang, X., Millman, J. S., Schub, O., Breitkreuz, K., Dewar, D., Rupes, I., Andrews, B., & Tyers, M. (2004). CDK activity antagonizes Whi5, an inhibitor of G1/S transcription in yeast. *Cell*, *117*(7), 899–913. https://doi.org/10.1016/j.cell.2004.05.024
- de Bruin, R. A., McDonald, W. H., Kalashnikova, T. I., Yates, J., 3rd, & Wittenberg, C. (2004). Cln3 activates G1-specific transcription via phosphorylation of the SBF bound repressor Whi5. *Cell*, *117*(7), 887–898. https://doi.org/10.1016/j.cell.2004.05.025
- Dietler, N., Minder, M., Gligorovski, V. *et al.* (2020). A convolutional neural network segments yeast microscopy images with high accuracy. *Nat Commun* 11, 5723. https://doi.org/10.1038/s41467-020-19557-4
- Edgington, N. P., & Futcher, B. (2001). Relationship between the function and the location of G1 cyclins in S. cerevisiae. *Journal of cell science*, *114*(Pt 24), 4599–4611. https://doi.org/10.1242/jcs.114.24.4599
- Egelhofer, T. A., Villén, J., McCusker, D., Gygi, S. P., & Kellogg, D. R. (2008). The septins function in G1 pathways that influence the pattern of cell growth in budding yeast. *PloS one*, *3*(4), e2022. https://doi.org/10.1371/journal.pone.0002022
- Ercan, D.P.; Chrétien, F.; Chakravarty, P.; Flynn, H.R.; Snijders, A.P.; Uhlmann, F. Budding yeast relies on G1 cyclin specificity to couple cell cycle progression with morphogenetic development. Sci. Adv. **2021**, 7, eabg0007.
- Fay, M. P.; Proschan, M. A. (2010). Wilcoxon–Mann–Whitney or t-test? On assumptions for hypothesis tests and multiple interpretations of decision rules. *Statistics Surveys*. **4**: 1–39. *doi*:*10.1214/09-SS051*
- Ferrezuelo, F., Colomina, N., Palmisano, A. *et al.* The critical size is set at a single-cell level by growth rate to attain homeostasis and adaptation. *Nat Commun* **3,** 1012 (2012). https://doi.org/10.1038/ncomms2015
- Fox, J. and Weisberg, S. (2019). An {R} Companion to Applied Regression, Third Edition. Thousand Oaks CA: Sage. URL: https://socialsciences.mcmaster.ca/jfox/Books/Companion/

- François-Lavet, V., Henderson, P., Islam, R., Bellemare, M. G. and Pineau, J. (2018), "An Introduction to Deep Reinforcement Learning", Foundations and Trends in Machine Learning: Vol. 11: No. 3-4, pp 219-354. http://dx.doi.org/10.1561/2200000071
- Gahan, P. B. (2005). The cell: a molecular approach (3rd edn) G. M. Cooper and R. E. Hausman, Palgrave-Macmillans Global Academic Publishing, 713 pp., ISBN 0–87893-214-3 (2004). *Cell Biochemistry and Function*, *23*(3), 222. https://doi.org/10.1002/cbf.1157
- Gladfelter, A. S., Kozubowski, L., Zyla, T. R., & Lew, D. J. (2005). Interplay between septin organization, cell cycle and cell shape in yeast. *Journal of Cell Science*, *118*(8), 1617–1628. https://doi.org/10.1242/jcs.02286
- Hartwell, L., & Weinert, T. (1989). Checkpoints: controls that ensure the order of cell cycle events. *Science*, *246*(4930), 629–634. https://doi.org/10.1126/science.2683079
- Kruskal W., Wallis, W. A. (1952). Use of ranks in one-criterion variance analysis. *Journal of the American Statistical Association*. **47** (260): 583–621. *doi*:*10.1080/01621459.1952.10483441*
- Lecun, Y., Bottou, L., Bengio, Y. and Haffner, P. (1998). "Gradient-based learning applied to document recognition". *Proceedings of the IEEE*, vol. 86, no. 11, pp. 2278-2324, doi: 10.1109/5.726791.
- McCusker, D., Denison, C., Anderson, S. *et al.* Cdk1 coordinates cell-surface growth with the cell cycle. *Nat Cell Biol* 9, 506–515 (2007). https://doi.org/10.1038/ncb1568
- Moffat, J., & Andrews, B. (2003). Late-G1 cyclin–CDK activity is essential for control of cell morphogenesis in budding yeast. *Nature Cell Biology*, *6*(1), 59–66. https://doi.org/10.1038/ncb1078
- Morgan, D. O. (2007). *The Cell Cycle: Principles of Control (Primers in Biology)* (1st edition). Sinauer Associates, Inc.
- Neurohr, G. E., Terry, R. L., Sandikci, A., Zou, K., Li, H., & Amon, A. (2018). Deregulation of the G1/S-phase transition is the proximal cause of mortality in old yeast mother cells. *Genes & Development*, *32*(15–16), 1075–1084. https://doi.org/10.1101/gad.312140.118
- Novarina, D., Koutsoumpa, A., and Milias-Argeitis, A., 2022. *A user-friendly and streamlined protocol for CRISPR/Cas9 genome editing in budding yeast*. STAR Protocols (to appear)
- Perrino, G., Napolitano, S., Galdi, F., La Regina, A., Fiore, D., Giuliano, T., Di Bernardo, M., & Di Bernardo, D. (2021). Automatic synchronisation of the cell cycle in budding yeast through closed-loop feedback control. *Nature Communications*, *12*(1). https://doi.org/10.1038/s41467-021-22689-w
- Queralt, E., & Igual, J. C. (2004). Functional distinction between Cln1p and Cln2p cyclins in the control of the Saccharomyces cerevisiae mitotic cycle. *Genetics*, *168*(1), 129–140. https://doi.org/10.1534/genetics.104.029587
- R Core Team (2021). R: A language and environment for statistical computing. R Foundation for Statistical Computing, Vienna, Austria. URL https://www.R-project.org/.
- Rullan, M., Benzinger, D., Schmidt, G. W., Milias-Argeitis, A., & Khammash, M. (2018). An Optogenetic Platform for Real-Time, Single-Cell Interrogation of Stochastic Transcriptional Regulation. *Molecular Cell*, *70*(4), 745–756.e6. https://doi.org/10.1016/j.molcel.2018.04.012
- Sha, W., Moore, J., Chen, K., Lassaletta, A. D., Yi, C. S., Tyson, J. J., & Sible, J. C. (2003). Hysteresis drives cell-cycle transitions in Xenopus laevis egg extracts. *Proceedings of the National Academy of Sciences of the United States of America*, *100*(3), 975–980. https://doi.org/10.1073/pnas.0235349100

- Skotheim, J. M., Di Talia, S., Siggia, E. D., & Cross, F. R. (2008). Positive feedback of G1 cyclins ensures coherent cell cycle entry. *Nature*, *454*(7202), 291–296. https://doi.org/10.1038/nature07118
- Steel, H., Habgood, R., Kelly, C. and Papachristodoulou, A. (2019). Chi.Bio: An open-source automated experimental platform for biological science research. https://doi.org/10.1101/796516.
- Treloar, N. J., Fedorec, A., Ingalls, B., & Barnes, C. P. (2020). Deep reinforcement learning for the control of microbial co-cultures in bioreactors. *PLoS computational biology*, *16*(4), e1007783. https://doi.org/10.1371/journal.pcbi.1007783
- Van Valen, D. A., Kudo, T., Lane, K. M., Macklin, D. N., Quach, N. T., DeFelice, M. M., Maayan, I., Tanouchi, Y., Ashley, E. A., & Covert, M. W. (2016). Deep Learning Automates the Quantitative Analysis of Individual Cells in Live-Cell Imaging Experiments. *PLoS computational biology*, *12*(11), e1005177. https://doi.org/10.1371/journal.pcbi.1005177
- Venkitaraman, A. R. (2002). Cancer Susceptibility and the Functions of BRCA1 and BRCA2. *Cell*, *108*(2), 171–182. https://doi.org/10.1016/s0092-8674(02)00615-3
- Wayne, D. W. (1990). Spearman rank correlation coefficient. *Applied Nonparametric Statistics* (2nd ed.). Boston: PWS-Kent. pp. 358–365. *ISBN 978-0-534-91976-4*
- Wickham, H. (2016). ggplot2: Elegant Graphics for Data Analysis. Springer-Verlag New York.
- Wickham, H., François, R., Henry, L. and Müller, K. (2021). dplyr: A Grammar of Data Manipulation. R package version 1.0.6. https://CRAN.R-project.org/package=dplyr
- Wittenberg, C., & Reed, S. I. (2005). Cell cycle-dependent transcription in yeast: promoters, transcription factors, and transcriptomes. *Oncogene*, *24*(17), 2746–2755. https://doi.org/10.1038/sj.onc.1208606
- Zoltowski, B. D., Motta-Mena, L. B., & Gardner, K. H. (2013). Blue Light-Induced Dimerization of a Bacterial LOV–HTH DNA-Binding Protein. Biochemistry, 52(38), 6653–6661. https://doi.org/10.1021/bi401040m